



Article

Study of $D_{s1}(2460)^+ \rightarrow D_s^+ \pi^+ \pi^-$ in $B \rightarrow \bar{D}^{(*)} D_s^+ \pi^+ \pi^-$ decays

LHCb collaboration #

ARTICLE INFO

Article history:

Received 7 November 2024

Received in revised form 21 December 2024

Accepted 22 January 2025

Available online 25 February 2025

Keywords:

LHCb experiment
Spectroscopy
Amplitude analysis
Low-energy QCD
B physics
Charm physics

ABSTRACT

An amplitude analysis of the $D_{s1}(2460)^+ \rightarrow D_s^+ \pi^+ \pi^-$ transition is performed simultaneously in $B^0 \rightarrow D^- D_s^+ \pi^+ \pi^-$, $B^+ \rightarrow \bar{D}^0 D_s^+ \pi^+ \pi^-$, and $B^0 \rightarrow D^{*-} D_s^+ \pi^+ \pi^-$ decays. The study is based on a data sample of proton-proton collisions recorded with the LHCb detector at centre-of-mass energies of $\sqrt{s} = 7, 8$, and 13 TeV, corresponding to a total integrated luminosity of 9 fb^{-1} . A clear double-peak structure is observed in the $m(\pi^+ \pi^-)$ spectrum of the $D_{s1}(2460)^+ \rightarrow D_s^+ \pi^+ \pi^-$ decay. The data can be described either with a model including $f_0(500)$, $f_0(980)$, and $f_2(1270)$ resonances, in which the contributions of $f_0(980)$ and $f_2(1270)$ are unexpectedly large, or with a model including $f_0(500)$, a doubly charged open-charm tetraquark state T_{cs}^{++} and its isospin partner T_{cs}^0 . If the former is considered implausible, the T_{cs} states are observed with high significance, and the data are consistent with isospin symmetry. When imposing isospin constraints between the two T_{cs} states, their mass and width are determined to be $(2327 \pm 13 \pm 13) \text{ MeV}$ and $(96 \pm 16_{-23}^{+170}) \text{ MeV}$, respectively, where the first uncertainty is statistical and the second is systematic. The mass is slightly below the DK threshold, and a spin-parity of 0^+ is favoured with high significance.

© 2025 The Authors. Published by Elsevier B.V. and Science China Press. This is an open access article under the CC BY license (<http://creativecommons.org/licenses/by/4.0/>).

1. Introduction

Since the observation of the $D_{s0}^*(2317)^+$ and $D_{s1}(2460)^+$ mesons in 2003 [1,2], their nature has been discussed extensively but without a firm conclusion [3–12]. The $D_{s0}^*(2317)^+$ and $D_{s1}(2460)^+$ masses are much lower than the expectation in the quark model [13–15]. The observed degeneracy between the masses of the charmed mesons ($D_{s0}^*(2300)^{0(\pm)}$ and $D_1(2430)^0$) and the charmed-strange mesons ($D_{s0}^*(2317)^\pm$ and $D_{s1}(2460)^\pm$) in the $(0^+, 1^+)$ doublet [16], indicates that the $D_{s0}^*(2317)^+$ and $D_{s1}(2460)^+$ states probably have nontrivial internal structure.¹ Due to their relatively small masses, their decays to $D^{(*)}K$ states are forbidden, resulting in total widths of a few MeV or less [17] and substantial branching fractions for the isospin-violating decays to $D_s^{(*)} \pi^0$ final states². The isospin-conserving decay, $D_{s1}(2460)^+ \rightarrow D_s^+ \pi^+ \pi^-$, also occurs at a sizeable rate [17,18]. Theoretical calculations predict a double-bump lineshape in the $\pi^+ \pi^-$ invariant-mass spectrum in this decay if the $D_{s1}(2460)^+$ meson is a $D^{(*)}K$ hadronic molecule [19].

The LHCb collaboration recently reported the observation of two neutral tetraquark states, labelled $T_{cs0}(2900)^0$ and

$T_{cs1}(2900)^0$, in $B^- \rightarrow D^+ D^- K^-$ decays [20,21]³. Later, LHCb also observed a doubly charged tetraquark and its neutral partner, labelled $T_{cs}(2900)^{++}$ and $T_{cs}(2900)^0$ with $I(J^P) = 1(0^+)$ where I denotes the isospin of the particle, in $B \rightarrow \bar{D} D_s^+ \pi$ decays [22,23].

The proximity of the masses of these states to the $D^* K^2$ threshold suggests that they might be $D^* K^*$ bound states [24–26]. Furthermore, recent theoretical work suggests that the multiplet including $T_{cs}(2900)^{++}$, $T_{cs}(2900)^0$, and $T_{cs0}(2900)^0$ tetraquarks could be the radial excitation of a lighter multiplet containing the $D_{s0}^*(2317)$ state [27]. If so, scalar DK bound states with isospin 1 near the DK threshold are also expected and the relationship between this triplet and the $D_{s0}^*(2317)^+$ state needs further clarification [28]. This motivates the study of three-body $D_{s1}(2460)^+$ decays to investigate the potential existence of $D_s \pi$ structures that may couple to the DK channel. Such research could shed new light on the internal structures of the $D_{s0}^*(2317)^+$ and $D_{s1}(2460)^+$ mesons.

In this paper, the results from a combined amplitude analysis of the $D_{s1}(2460)^+ \rightarrow D_s^+ \pi^+ \pi^-$ transition in $B^0 \rightarrow D^- D_s^+ \pi^+ \pi^-$, $B^+ \rightarrow \bar{D}^0 D_s^+ \pi^+ \pi^-$, and $B^0 \rightarrow D^{*-} D_s^+ \pi^+ \pi^-$ decays are presented. The study is based on a data sample of proton-proton (pp) collisions recorded with the LHCb detector at centre-of-mass energies of $\sqrt{s} = 7, 8$, and 13 TeV, corresponding to a total integrated luminosity of 9 fb^{-1} . The use of fully reconstructed B -meson decays

Authors are listed at the end of this paper.

¹ The form J^P denotes the total spin J and parity P .

² Natural units in which $c = \hbar = 1$ are used throughout the article.

³ The inclusion of charge-conjugate processes is implied throughout the article.

allows kinematic constraints on the decay chain to be applied, which improves the resolution, suppresses background contributions and enables the determination of the quantum numbers that affect the decay amplitudes.

2. Detector and simulation

The LHCb detector [29,30] is a single-arm forward spectrometer covering the pseudorapidity range $2 < \eta < 5$, designed for the study of particles containing b or c quarks. The detector includes a high-precision tracking system consisting of a silicon-strip vertex detector surrounding the pp interaction region, a large-area silicon-strip detector located upstream of a dipole magnet with a bending power of about 4 Tm, and three stations of silicon-strip detectors and straw drift tubes placed downstream of the magnet. The tracking system provides a measurement of the momentum, p , of charged particles with a relative uncertainty that varies from 0.5% at low momentum to 1.0% at 200 GeV. The minimum distance of a track to a primary pp collision vertex (PV), the impact parameter (IP), is measured with a resolution of $(15 + 29/p_T) \mu\text{m}$, where p_T is the component of the momentum transverse to the beam, in GeV. Different types of charged hadrons are distinguished using information from two ring-imaging Cherenkov detectors.

In this analysis, the online selections include hardware and software triggers. The hardware trigger criteria are satisfied by energy deposits in the calorimeter associated with the signal candidate decay. The software trigger requires a two-, three- or four-track secondary vertex with significant displacement from any primary pp interaction vertex. In general, at least one charged particle must have a transverse momentum $p_T > 1.6$ GeV and be inconsistent with originating from a PV.

Simulation is required to determine the detector efficiency (which includes the detector acceptance and selection requirements). In the simulation, pp collisions are generated using PYTHIA [31,32] with a specific LHCb configuration [33]. Decays of unstable particles are described by EVTGEN [34], in which final-state radiation is generated using PHOTOS [35]. The interaction of the generated particles with the detector, and its response, are implemented using the GEANT4 toolkit [36,37] as described in Ref. [38]. The underlying pp interaction is reused multiple times using REDECAY [39], with an independently generated signal decay for each interaction.

3. Selection

The intermediate $D_{s1}(2460)^+$, D^{*-} , D_s^+ , \bar{D}^0 , and D^- mesons are reconstructed through the following decays: $D_{s1}(2460)^+ \rightarrow D_s^+ \pi^+ \pi^-$, $D^{*-} \rightarrow \bar{D}^0 \pi^-$, $D_s^+ \rightarrow K^- K^+ \pi^+$, $\bar{D}^0 \rightarrow K^+ \pi^-$, and $D^- \rightarrow K^+ \pi^- \pi^-$. The charged K and π candidates are formed from well-reconstructed tracks that are inconsistent with originating from any PV, with particle identification information consistent with the corresponding mass hypothesis. The D_s^+ , \bar{D}^0 , and D^- candidates are required to have good vertex quality and significant displacement with respect to all PVs. Combinatorial background is suppressed with requirements on the outputs of trained boosted decision tree (BDT) classifiers [40–43], which take as input transverse momentum, tracking, vertexing and particle identification variables. Each BDT classifier is trained with simulated D mesons from B decays as signal and combinatorial background from mass sideband regions in data. The mass of the reconstructed candidates must be within ± 15 MeV of the corresponding known mass⁴. The $D_{s1}(2460)^+$ and D^{*-} candidates are formed from combinations of

charged pions with D_s^+ and \bar{D}^0 candidates, respectively, where the combined vertices must be of good quality and displaced from all PVs. The mass difference between the D^{*-} candidate and its \bar{D}^0 decay product is required to be less than 150 MeV. The reconstructed $D_{s1}(2460)^+$ candidate mass must be less than 2700 MeV for the fit to the $m(D_s^+ \pi^+ \pi^-)$ invariant-mass distribution used to determine the signal and background yields, and must be within ± 10 MeV of its known value for the subsequent amplitude fit.

The B candidates are formed by combining a $\bar{D}^{(*)}$ and a $D_{s1}(2460)^+$ candidate, and requiring a well-reconstructed vertex which is displaced from all PVs. The momentum vector of each B candidate is required to point back to the PV where it is hypothesised to have been produced, referred to hereafter as the associated PV. The reconstructed B -meson mass is required to be within ± 20 MeV of its known value. For the $B^+ \rightarrow \bar{D}^0 D_{s1}(2460)^+$ signal channel, an additional requirement that the $\bar{D}^0 \pi^-$ invariant-mass be larger than 2020 MeV is applied to veto potential D^{*-} background contamination. After applying the selection criteria, around 5% of the remaining events contain more than one B candidate; in these cases, only one is kept randomly.

Kinematic fits [44] are used at different stages of the data analysis. By default, the B candidate is constrained to have originated from the associated PV. When considering the B -candidate mass distribution, further constraints on the masses of the $\bar{D}^{(*)}$ and D_s^+ candidates to their known values are applied. For the invariant-mass fit described in the next section, in addition to the above constraints, the B -candidate mass is fixed in the kinematic fit to its known value to improve the $D_{s1}(2460)^+$ mass resolution. Finally, an additional $D_{s1}(2460)^+$ mass constraint is applied in the fit used to obtain the four-momenta of the final-state particles for the amplitude analysis. This is valid since the small $D_{s1}(2460)^+$ width [17] has negligible impact on the analysis.

4. Invariant-mass fit

The $m(D_s^+ \pi^+ \pi^-)$ invariant-mass spectra for the three signal channels after all selection criteria are shown in Fig. 1. Clear $D_{s1}(2460)^+$ signals are observed in all three channels, together with a smoothly varying combinatorial background and a small contribution from $D_{s1}(2536)^+ \rightarrow D_s^+ \pi^+ \pi^-$ decays. Extended unbinned maximum-likelihood fits the data, where the lower bound is the kinematic threshold $m_{D_s^+} + 2m_{\pi^+}$, are performed to extract signal and background yields for the subsequent amplitude fit. The $D_{s1}(2460)^+$ and $D_{s1}(2536)^+$ components are modelled by relativistic Breit-Wigner (RBW) functions [16] convolved with a common Gaussian function to account for experimental resolution. The $D_{s1}(2460)^+$ Breit-Wigner mass and width are free to vary in the fit while the $D_{s1}(2536)^+$ parameters are fixed to their known values. The width of the Gaussian resolution function is shared between the $D_{s1}(2460)^+$ and $D_{s1}(2536)^+$ components and is allowed to vary in the fit. The combinatorial background is modelled by an ARGUS function [45] with the fixed kinematic threshold of 2247 MeV and the shape parameter governing the slope is free to vary in the fit.

The fit results for the three signal channels are shown together with the data distributions in Fig. 1. The signal and background yields inside the signal region, defined to be ± 5 MeV around the $D_{s1}(2460)^+$ known mass, are summarised in Table 1. In total around 800 signal events are obtained.

5. Amplitude analysis formalism

The amplitudes of the signal decays are expressed using the helicity formalism with an isobar approach [46–48], where the total

⁴ Unless otherwise specified, known values of particle properties are taken from Ref. [16].

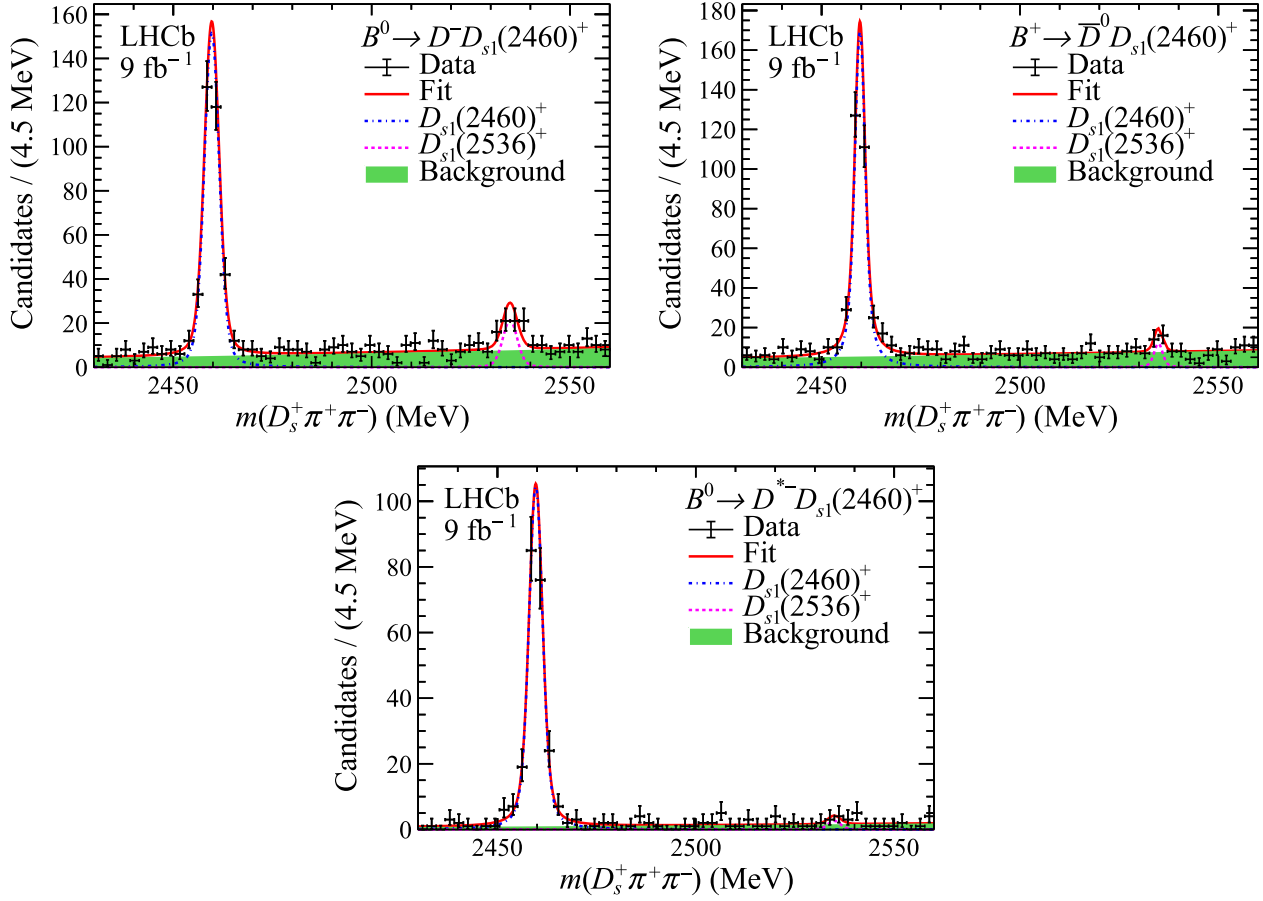


Fig. 1. Invariant-mass distributions for the $D_{s1}(2460)^+$ candidates in the three signal channels (black dots with error bars) shown with the fit model (solid lines). The coloured region shows the combinatorial background.

Table 1

Estimated signal and background yields inside the $D_{s1}(2460)^+$ mass window, together with the signal fraction^a.

Channel	Signal yield	Background yield	Signal fraction (%)
$B^0 \rightarrow D^- D_s^+ \pi^+ \pi^-$	305 ± 20	22 ± 1	93.2 ± 0.4
$B^+ \rightarrow \bar{D}^0 D_s^+ \pi^+ \pi^-$	279 ± 18	24 ± 1	92.2 ± 0.5
$B^0 \rightarrow D^{*-} D_s^+ \pi^+ \pi^-$	205 ± 14	4 ± 1	98.0 ± 0.2

^a Note that the extrapolation of the background yield into the signal window allows uncertainties on the yields (N) to be smaller than \sqrt{N} .

amplitude is a coherent sum of quasi-two-body amplitudes. The Blatt-Weisskopf factor in the amplitudes is fixed to 3.0GeV^{-1} in the amplitude fit. Each resonant lineshape is modelled by a RBW function, if not specified otherwise. The $f_0(980)$ state is modelled by a modified Flatté function [49,50], with its parameters fixed according to Refs. [50,51]. The K -matrix model suggested in Refs. [52,53] is used as an alternative $\pi\pi$ S-wave lineshape. Due to the small phase space available in $D_{s1}(2460)^+ \rightarrow D_s^+ \pi^+ \pi^-$ decays, the accessible $m(\pi\pi)$ range is limited and the analysis has little sensitivity to the parameters related to the $K\bar{K}$, 4π , $\eta\eta$, and $\eta\eta'$ coupled channels; such parameters are fixed to zero in the fit.

An alternative model for $\pi\pi$ lineshapes, based on the assumption of the $D_{s1}(2460)^+$ meson being a compact or a molecular state [19] and hereafter referred to as the chiral dynamics model, is also tested. This model includes separate compact and molecular components, each obtained using a two-dimensional interpolation of the $\cos\theta_1$ (defined below) and $m(\pi^+ \pi^-)$ distributions from the data points provided in Ref. [19], with relative fractions set by a parameter that is determined in the fit.

Another K -matrix model based on the scattering length approximation, considering DK and $D_s\pi$ coupled-channel effects, is used as a possible lineshape to describe $T_{c\bar{s}}$ states. Details of this model can be found in the review of resonances in Ref. [16] and also in Ref. [54]. The scattering K -matrix is parameterised as

$$K = \begin{pmatrix} \gamma & \beta \\ \beta & \gamma_2 \end{pmatrix}, \quad (1)$$

where γ is proportional to the scattering length in the elastic DK channel, β describes the coupling to the inelastic $D_s\pi$ channel, and γ_2 includes the possible interaction in the $D_s\pi$ channel. The lineshape for the $D_s\pi$ decay is

$$f^{K\text{-matrix}} = \frac{\beta^2 \rho_{DK} + i\gamma_2(i\gamma\rho_{DK} - 1)}{\beta^2 \rho_{DK}\rho_{D_s\pi} + (i\gamma\rho_{DK} - 1)(i\gamma_2\rho_{D_s\pi} - 1)}, \quad (2)$$

and the scattering length is

$$a = \frac{1}{8\pi\sqrt{s_{\text{thr}}}} (\gamma + i\beta^2 \rho_{D_s\pi}(s_{\text{thr}})), \quad (3)$$

where $s_{\text{thr}} = (m_D + m_K)^2$, and $\rho_{DK/D_s\pi}$ denotes the dimensionless phase-space term. The parameter γ_2 is fixed to zero in the amplitude fit, since there is little sensitivity to it in the channels under study.

An unbinned maximum-likelihood fit is performed simultaneously to the three signal channels. The negative log-likelihood function for each channel is defined as

$$-\ln \mathcal{L} = - \sum_{i \in \text{data}} \ln [f_{\text{sig}} \mathcal{P}_{\text{sig}}(\xi_i; \Lambda) + (1 - f_{\text{sig}}) \mathcal{P}_{\text{bkg}}(\xi_i; \Lambda)], \quad (4)$$

where f_{sig} denotes the signal fraction in the signal region, determined from the $m(D_s^+ \pi^+ \pi^-)$ fit described previously. The term \mathcal{P}_{sig} stands for the signal probability density function (PDF) for candidate i at position ξ_i in phase space,

$$\mathcal{P}_{\text{sig}}(\xi_i; \Lambda) = \frac{|A(\xi_i; \Lambda)|^2}{\int |A(\xi; \Lambda)|^2 \varepsilon(\xi) d\xi}, \quad (5)$$

where Λ denotes the set of parameters to be determined in the fit to data. Here, A is the total amplitude and $\varepsilon(\xi)$ denotes the efficiency variation over the phase space, which is determined from simulated samples after applying simulation corrections on the tracking and trigger efficiencies, obtained using control samples [55,56]. The masses and widths of the considered resonances and their coupling constants are shared between the three channels. The background PDF $\mathcal{P}_{\text{bkg}}(\xi_i; \Lambda)$ is estimated using events in the $m(D_s^+ \pi^+ \pi^-)$ sidebands [2247, 2440] MeV and [2560, 2660] MeV, and is described using kernel density estimation [57].

The results of the amplitude analysis are expressed in terms of fit fractions. The fit fraction F_i for resonance i is calculated based on the fitted values of the parameters $\hat{\Lambda}$, and is defined as

$$F_i = \frac{\int |A_i(\xi; \hat{\Lambda})|^2 d\xi}{\int |\sum_k A_k(\xi; \hat{\Lambda})|^2 d\xi}, \quad (6)$$

where $A_i(\xi)$ is the contribution to the amplitude from resonance i . The interference between any two components i and j , F_{ij} , is quantified as

$$F_{ij} = \frac{\int 2 \text{Re} \{ A_i A_j^*(\xi; \hat{\Lambda}) \} d\xi}{\int |\sum_k A_k(\xi; \hat{\Lambda})|^2 d\xi}. \quad (7)$$

6. Amplitude fit

Fig. 2 shows the distributions of selected candidates in the $m(D_s^+ \pi^+) - m(\pi^+ \pi^-)$ and $\phi_1 - \cos \theta_1$ planes, combining the $B^0 \rightarrow D^- D_{s1}(2460)^+$ and $B^+ \rightarrow \bar{D}^0 D_{s1}(2460)^+$ channels. These four variables fully describe the dynamics of the two included decays, while in the $B^0 \rightarrow D^- D_{s1}(2460)^+$ case two additional angles related to D^{*-} decays are necessary, making it inappropriate to combine

the three distributions. The variable θ_1 is the helicity angle of the $R(\pi\pi)$ resonance in $D_{s1}(2460)^+ \rightarrow D_s^+ R(\pi\pi)$ decays and ϕ_1 is the angle between the decay planes of $D_{s1}(2460)^+ \rightarrow D_s^+ R(\pi\pi)$ and $R(\pi\pi) \rightarrow \pi^+ \pi^-$ decays. Complete definitions of the angles are shown in Fig. S1 in the Supplementary material. Efficiency-corrected one-dimensional projections onto each of the phase-space variables, including $m(D_s^+ \pi^-)$ which is expected to be consistent with $m(D_s^+ \pi^+)$ due to isospin symmetry, are shown in Figs. S2 and S3 in the Supplementary material. The data cluster in three phase-space regions, two of which are seen as a double bump in the $m(D_s^+ \pi^+)$ distribution when requiring $m(\pi^+ \pi^-) > 0.39$ GeV, as shown in Fig. 3(c) for example. The corresponding distributions for $B^0 \rightarrow D^{*-} D_{s1}(2460)^+$ decays and projections on the efficiency-corrected $m(\pi^+ \pi^-)$, $m(D_s^+ \pi^+)$, $\cos \theta_1$, and ϕ_1 distributions for the three channels are shown in the Supplementary material.

In the $D_{s1}(2460)^+ \rightarrow D_s^+ \pi^+ \pi^-$ decays, conventional quark-antiquark resonances are only possible in the $\pi\pi$ channel. Therefore, models with only $\pi\pi$ resonances are attempted first.

A summary of the relative negative log likelihoods (ΔNLL) for different models containing only $\pi\pi$ resonances is given in the upper section of Table 2. When considering only $\pi\pi$ resonance contributions, two models give the best description of the data without adding nonsignificant resonant contributions. One contains the $f_0(500)$, $f_0(980)$, and $f_2(1270)$ states, and the other describes the $\pi\pi$ S-wave with a K -matrix component and includes an additional $f_2(1270)$ resonance. The projections onto $m(\pi^+ \pi^-)$, $m(D_s^+ \pi^+)$, and $m(D_s^+ \pi^-)$ requiring $m(\pi^+ \pi^-) > 0.39$ GeV for the first model are shown in Fig. 3. The corresponding $m(\pi^+ \pi^-) - m(D_s^+ \pi^+)$ and $\phi_1 - \cos \theta_1$ distributions are shown in Fig. S5 in the Supplementary material. The inclusion of the $f_2(1270)$ component is necessary to obtain good agreement with the data. The fits with models excluding this component have much higher ΔNLL values, as seen in Table 2. The inclusion of a $\rho(770)^0$ component leads to a small improvement in ΔNLL , but this is insignificant bearing in mind the change in the number of free parameters of the fit.

Although these models give reasonable descriptions of the data across the $D_{s1}(2460)^+ \rightarrow D_s^+ \pi^+ \pi^-$ phase space, there are several reasons to doubt their credibility as physical descriptions of the decay amplitude. Firstly, there is a large contribution from the $f_2(1270)$ resonance, despite the fact that the kinematic upper limit

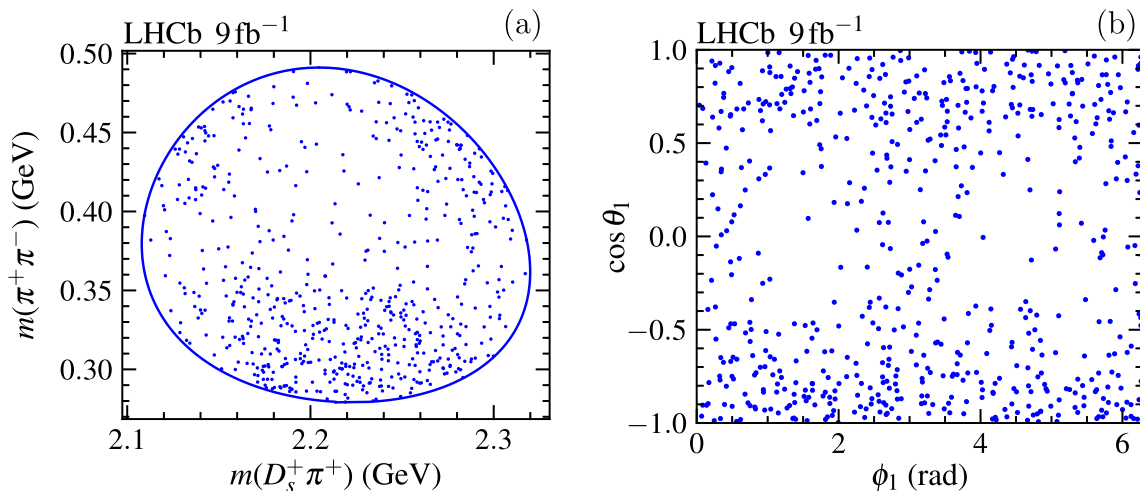


Fig. 2. Distributions of selected candidates in the (a) $m(D_s^+ \pi^+) - m(\pi^+ \pi^-)$ plane and (b) $\phi_1 - \cos \theta_1$ plane, combining the $B^0 \rightarrow D^- D_{s1}(2460)^+$ and $B^+ \rightarrow \bar{D}^0 D_{s1}(2460)^+$ channels. The blue solid line in (a) denotes the boundary of the $D_{s1}(2460)^+ \rightarrow D_s^+ \pi^+ \pi^-$ Dalitz plot. Background contributions are not subtracted and no efficiency corrections are applied.

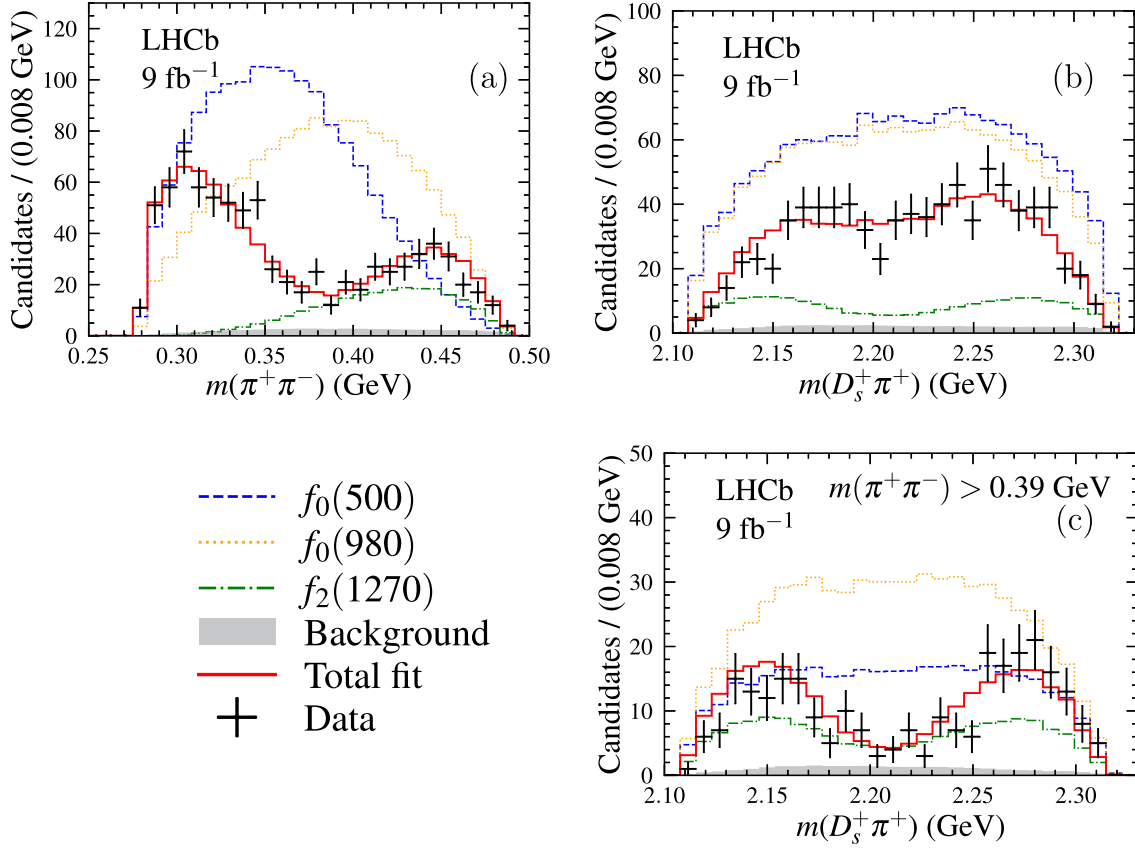


Fig. 3. Comparison between data (black dots with error bars) and results of the fit with the $f_0(500) + f_0(980) + f_2(1270)$ model (red solid line). The distributions are for the three channels combined in (a) $m(\pi^+\pi^-)$, (b) $m(D_s^+\pi^+)$, and (c) $m(D_s^+\pi^+)$ requiring $m(\pi^+\pi^-) > 0.39$ GeV. Individual components, corresponding to the background contribution estimated from $m(D_s^+\pi^+)$ sideband regions (gray-filled) and the different resonant contributions (coloured dashed lines), are also shown as indicated in the legend.

Table 2

Relative negative log likelihoods (Δ NLL) and numbers of fit parameters for all tested models^a.

Model	Δ NLL	Number of fit parameters
Chiral dynamics	177.8	5
K -matrix $\pi\pi$ S-wave	249.0	6
$f_0(500) + f_0(980)$	245.2	8
$f_0(500) + f_0(980) + \rho(770)^0$	148.0	12
$f_0(500) + f_0(980) + f_2(1270)$	3.7	12
$f_0(500) + f_0(980) + f_2(1270) + \rho(770)^0$	-2.8	16
K -matrix $\pi\pi$ S-wave + $f_2(1270)$	5.9	10
$f_0(500) + \text{RBW } T_{\text{CS}}(0^+)$	3.5	10
$f_0(500) + K\text{-matrix } T_{\text{CS}}(0^+)$	0.0	10
$f_0(500) + f_0(980) + \text{RBW } T_{\text{CS}}(0^+)$	-3.0	12
$f_0(500) + \rho(770)^0 + \text{RBW } T_{\text{CS}}(0^+)$	-1.1	14
$f_0(500) + f_2(1270) + \text{RBW } T_{\text{CS}}(0^+)$	-4.3	14
$f_0(500) + \text{RBW } T_{\text{CS}}(1^-)$	62.9	12

^a The Δ NLL value is calculated with the model $f_0(500) + K\text{-matrix } T_{\text{CS}}(0^+)$ as reference. Smaller values of Δ NLL correspond to better fits. The upper section is for models containing only $\pi\pi$ resonances, while the lower section is for models with T_{CS} contributions.

of $m(\pi^+\pi^-)$ is around $m_{f_2(1270)} - 4 \cdot \Gamma_{f_2(1270)}$, where $m_{f_2(1270)}$ and $\Gamma_{f_2(1270)}$ are the known $f_2(1270)$ mass and width. Such a large contribution from the tail of a lineshape is barely plausible. A similar argument applies to the $f_0(980)$ contribution. Secondly, the model including both $f_0(500)$ and $f_0(980)$ components requires large destructive interference to generate the observed $m(\pi^+\pi^-)$ structures, with the total fit fraction summing to $(413 \pm 66)\%$. While

large interference effects are inevitable in an amplitude analysis with broad components overlapping in a small phase space, the dramatic effects seen here are markedly different from what is seen in $\pi\pi$ S-waves in other processes [51,58–64]. Furthermore, as shown in Table 3, the fitted value of the $f_0(500)$ mass, and to a lesser extent also that of its width, are different from what is seen in other processes [16].

In addition to the results shown above, some fits with the $f_0(500)$, $f_0(980)$, and $f_2(1270)$ states converge to another solution with a similar Δ NLL value. This solution, however, has a very large interference between the $f_0(500)$ and $f_0(980)$ resonances leading to unstable results. This solution also finds the $f_0(500)$ mass to be even smaller (around 190 MeV) and the $f_0(500)$ width larger than 700 MeV. It is not discussed further.

Due to these unsatisfactory aspects of the fit results for models containing only $\pi^+\pi^-$ resonances, models with additional exotic states decaying to $D_s^+\pi^\pm$, referred to as T_{CS}^{++} and T_{CS}^0 states, are considered. In all cases, both the T_{CS}^{++} and T_{CS}^0 isospin partners are included, and by default their coupling constants, masses and widths (or parameters β and γ for the K -matrix model) are constrained to be the same following isospin symmetry.

As seen in the lower section of Table 2, models with only $f_0(500)$ and T_{CS} states with spin-parity $J^P = 0^+$ give approximately as good descriptions of the data as the best (but, as discussed above, arguably implausible) models without T_{CS} states. Two possible T_{CS} lineshapes, RBW and K -matrix, are considered and give similar fit quality. The projections of the fit results are given in Figs. 4 and 5. The corresponding plots in the $m^2(\pi^+\pi^-) - m^2(D_s^+\pi^+)$ and $\phi_1 - \cos(\theta_1)$ planes with the RBW and K -matrix models are shown

Table 3
Summary of fit results for different models described in detail^{a)}.

Model	Resonance	Mass (MeV)	Width (MeV)	Fractions (%)
$f_0(500) + f_0(980) + f_2(1270)$	$f_0(500)$	$376 \pm 9 \pm 16$	$175 \pm 23 \pm 16$	$197 \pm 35 \pm 23$
	$f_0(980)$	945.5	167	$187 \pm 38 \pm 43$
	$f_2(1270)$	1275.4	186.6	$29 \pm 2 \pm 1$
$f_0(500) + \text{RBW } T_{c\bar{s}}(0^+)$	$f_0(500)$	$464 \pm 23 \pm 14$	$214 \pm 28 \pm 8$	$199^{+42}_{-47} \pm 39$
	$T_{c\bar{s}}^{++}/T_{c\bar{s}}^0$	$2312 \pm 27 \pm 11$	$264 \pm 46 \pm 21$	$126^{+27}_{-17} \pm 20$
$f_0(500) + K\text{-matrix } T_{c\bar{s}}(0^+)$	$f_0(500)$	$474 \pm 30 \pm 18$	$224 \pm 23 \pm 16$	$248^{+40}_{-54} \pm 39$
	$T_{c\bar{s}}^{++}/T_{c\bar{s}}^0$	$2327 \pm 13 \pm 13$	$96 \pm 16 \pm 23$	$156^{+27}_{-38} \pm 25$

^a Values quoted without uncertainties are taken from previous measurements [16,51] and are fixed in the fits. The two sources of uncertainty are statistical and systematic. For the models containing $T_{c\bar{s}}$ states the quoted fit fraction is the value for each of the isospin partners, and the quoted $T_{c\bar{s}}$ mass and width parameters are the pole mass and width.

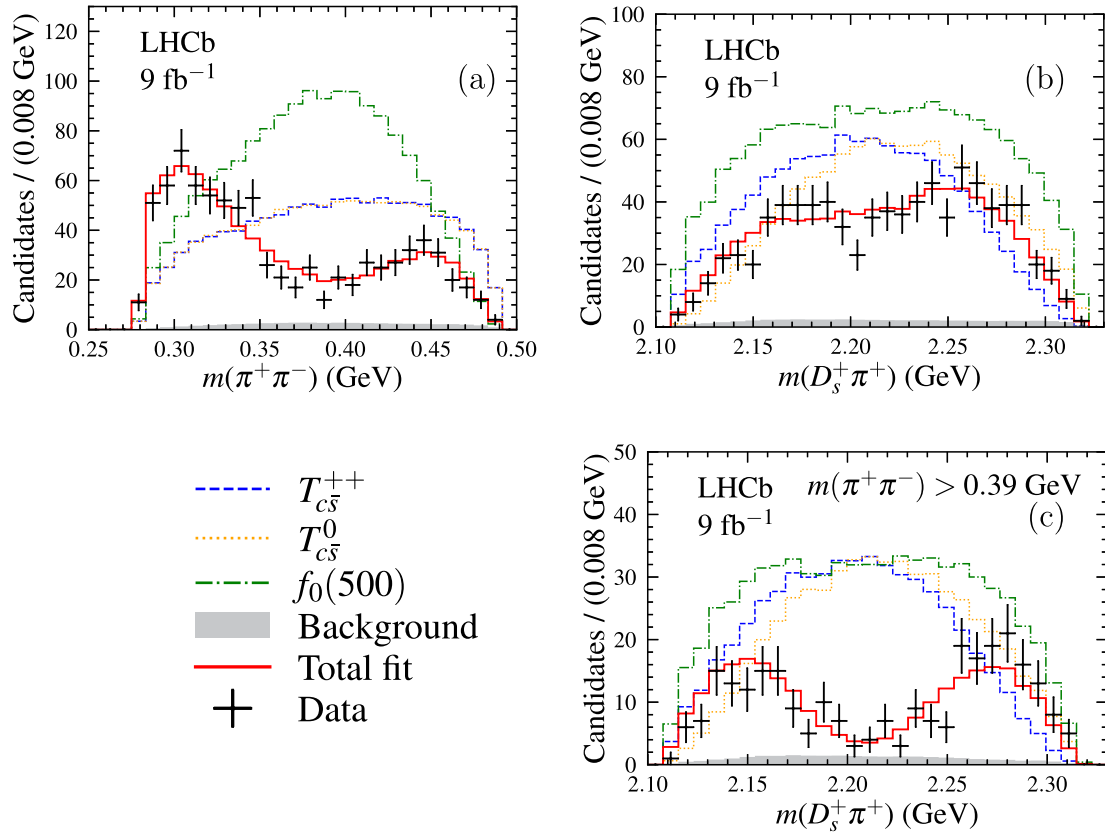


Fig. 4. Comparison between data (black dots with error bars) and results of the fit with the $f_0(500) + \text{RBW } T_{c\bar{s}}(0^+)$ model. The distributions are for the three channels combined in (a) $m(\pi^+\pi^-)$, (b) $m(D_s^+\pi^+)$, and (c) $m(D_s^+\pi^+)$ requiring $m(\pi^+\pi^-) > 0.39 \text{ GeV}$. Individual components, corresponding to the background contribution estimated from $m(D_s^+\pi^+)$ sideband regions (gray-filled) and the different resonant contributions (coloured dashed lines), are also shown as indicated in the legend.

in Figs. S6 and S7, respectively, in the Supplementary material. A second solution with similar ΔNLL is also obtained, but is quite unstable and therefore is not discussed further.

As seen from the large fit fractions in Table 3, fits with these models have similarly large destructive interference effects as in models without the $T_{c\bar{s}}$ states. It may also be noted that the fitted $f_0(500)$ mass and width values are now in better agreement with previous measurements [16]. The mass of the $T_{c\bar{s}}$ states is comparable between the RBW and K -matrix models but a large variation in the width is found. For the K -matrix model, the γ_2 parameter in Eq. (1) is fixed to 0 as it is expected that the coupling to the $D_s\pi$ channel is weak. Values of $\beta = 153 \pm 12$ and $\gamma = -259 \pm 21$ are obtained, from which the scattering length is calculated to be $-0.86(\pm 0.07) + 0.44(\pm 0.07)i \text{ fm}$, incompatible with the value predicted in Ref. [65]. The mass and width of the K -matrix model

given in Table 3 are calculated in the second Riemann sheet and are also different from those predicted in Ref. [66]. When allowed to vary freely in the fit, $\gamma_2 = 47 \pm 41$ is obtained, consistent with the expectation of zero, while $\beta = 133 \pm 16$ and $\gamma = -244 \pm 17$ are consistent with the values obtained when γ_2 is fixed to 0. The Argand diagrams [16] for the RBW and K -matrix descriptions of the $T_{c\bar{s}}$ lineshape are shown in Fig. 6, and are seen to be consistent with each other.

In order to test the assumption of isospin symmetry, the coupling constants, masses, and widths of the two $T_{c\bar{s}}$ states are allowed to differ. This is done in both the RBW and K -matrix $T_{c\bar{s}}$ models, with results consistent with isospin symmetry in both cases. For example, with the K -matrix $T_{c\bar{s}}$ lineshape, the mass and width for $T_{c\bar{s}}^{++}$ ($T_{c\bar{s}}^0$) are measured to be $2325 \pm 11 \text{ MeV}$ ($2325 \pm 10 \text{ MeV}$) and $81 \pm 14 \text{ MeV}$ ($118 \pm 20 \text{ MeV}$), respectively.

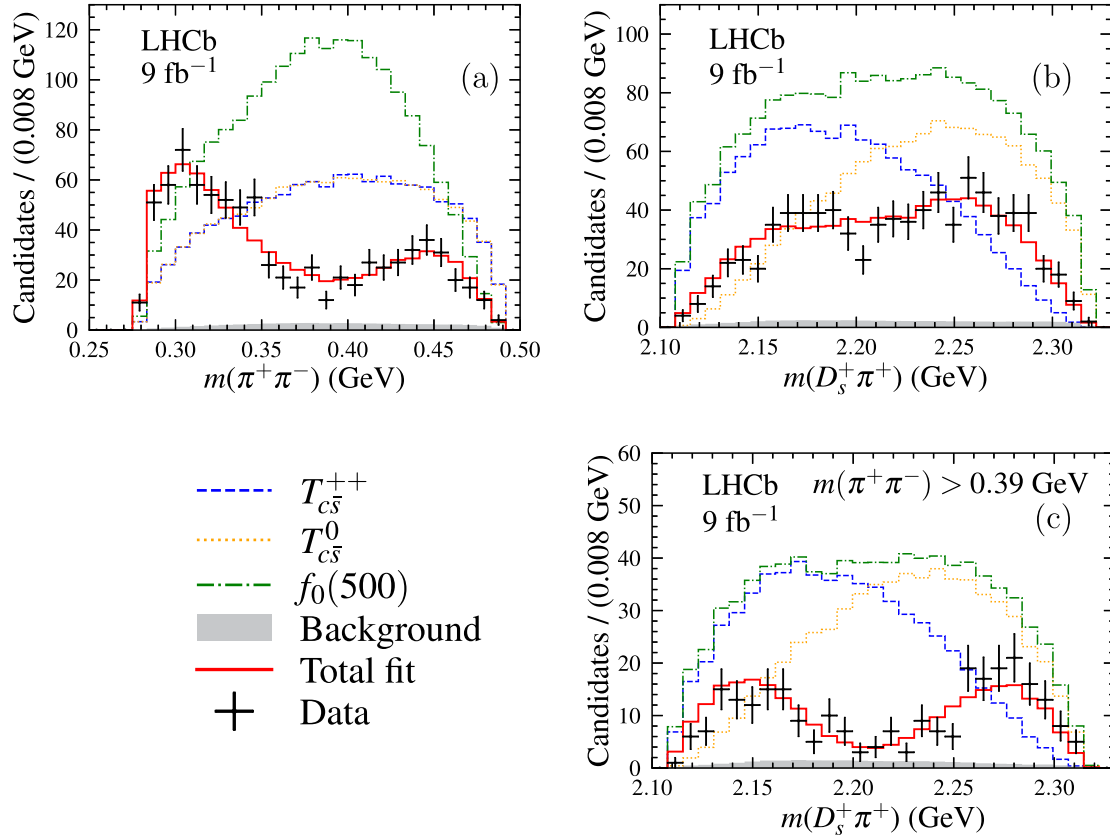


Fig. 5. Comparison between data (black dots with error bars) and results of the fit with the $f_0(500) + K$ -matrix $T_{c\bar{s}}(0^+)$ model (red solid line). The distributions are for the three channels combined in (a) $m(\pi^+\pi^-)$, (b) $m(D_s^+\pi^+)$, and (c) $m(D_s^+\pi^+)$ requiring $m(\pi^+\pi^-) > 0.39$ GeV. Individual components, corresponding to the background contribution estimated from $m(D_s^+\pi^+)$ sideband regions (gray-filled) and the different resonant contributions (coloured dashed lines), are also shown as indicated in the legend.

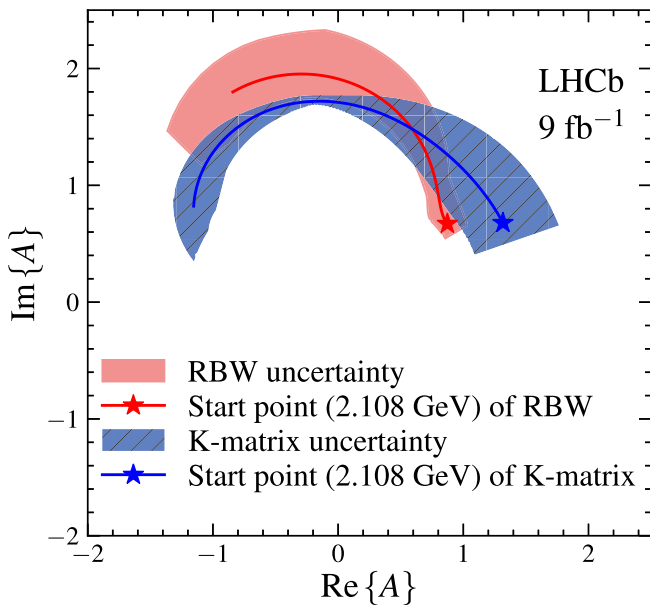


Fig. 6. Argand diagrams for the variation with mass of the $T_{c\bar{s}}$ states amplitude with both RBW and K -matrix models. The red and blue stars denote the lower $m(D_s\pi)$ kinematic limit (denoted “start point”). The statistical uncertainties for the RBW and K -matrix models are marked as red solid and blue slashed bands, respectively.

Models with additional $\rho(770)^0$, $f_0(980)$, and $f_2(1270)$ components are also tested. None of these extra contributions are found

to be significant, as seen in Table 2. An upper limit on the fit fraction of the isospin-breaking $D_{s1}(2460)^+ \rightarrow D_s^+\rho(770)^0$ decay is set at 2.8% at the 90% confidence level. This is less restrictive than the upper limit of 1.7% at the 90% confidence level obtained if the model does not include any $T_{c\bar{s}}$ component. Bearing in mind the large contributions from the $f_0(980)$ and $f_2(1270)$ components in the $f_0(500) + f_0(980) + f_2(1270)$ model, it is interesting to note that the corresponding contributions are small and not significant in the $f_0(500) + f_0(980) + T_{c\bar{s}}$ and $f_0(500) + f_0(1270) + T_{c\bar{s}}$ models. An attempt is made to fit with the $\pi\pi$ resonances described by the chiral dynamics model together with $T_{c\bar{s}}$ states, but the fit results have unphysically large interference and are not further discussed.

To estimate the significance of the two $T_{c\bar{s}}$ contributions, samples of pseudoexperiments are generated based on the results of the fit with a model containing $f_0(500)$ and $f_0(980)$ resonances only. These pseudoexperiments are each fitted both with and without $T_{c\bar{s}}$ states. The distribution of the $2\Delta\text{NLL}$ values between the two fit results is fitted with a χ^2 distribution, and the number of degrees of freedom (N_{dof}) is determined to be 6.77 ± 0.25 . Given that the $2\Delta\text{NLL}$ value from data is 490.4, the significance is estimated to be much larger than 10 standard deviations (σ). The $2\Delta\text{NLL}$ distribution is shown in Fig. S8 in the Supplementary material. This significance value implicitly rejects the $f_0(500) + f_0(980) + f_2(1270)$ model. If the null hypothesis is based on that model, the $T_{c\bar{s}}$ components are not significant.

The spin-parity of the $T_{c\bar{s}}$ states used in the fits is changed to 1^- instead of 0^+ . This reduces significantly the interference effects, but results in a ΔNLL value about 60 units larger than that obtained

with $J^P = 0^+ T_{c\bar{s}}$ states. Pseudoexperiments are generated according to the fit results under this alternative spin-parity assumption to evaluate the significance of this outcome. The pseudoexperiments are fitted with both spin-0 and spin-1 models, and the distribution of $2\Delta\text{NLL}$ values is obtained. Compared with the $2\Delta\text{NLL}$ value observed in data, the spin-parity 0^+ is favoured with 10σ significance. The $2\Delta\text{NLL}$ distribution is shown in Fig. S9 in the Supplementary material.

7. Systematic uncertainties

Systematic uncertainties are evaluated on the masses, widths and fit fractions of each of the components included in the $f_0(500) + f_0(980) + f_2(1270)$, $f_0(500) + \text{RBW } T_{c\bar{s}}(0^+)$, and $f_0(500) + K\text{-matrix } T_{c\bar{s}}(0^+)$ models. The sources of systematic uncertainty are divided into five categories: the signal fraction, the background model, the efficiency map, the fixed parameters in the amplitude fit, and the choices for the lineshape models. Among them, the dominant systematic uncertainties are from the fixed parameters in the amplitude fit and the choices for lineshape models. The total systematic uncertainties presented in Table 3 are determined by combining all contributions in quadrature, and do not include the uncertainty from the choices for the $T_{c\bar{s}}$ lineshape models, which is treated later.

Most of the systematic uncertainties are estimated by performing several times the fit to data, each time varying the input parameters within their respective uncertainties, such as altering distributions or fixed parameters. The root mean squares of the distributions of the fit results are taken as the corresponding measures of systematic uncertainty. A further source of uncertainty related to the signal fraction is estimated by changing the signal shape in the $m(D_s^+ \pi^+ \pi^-)$ fit to a Gaussian function and calculating the resulting signal fraction. The difference between the results in the amplitude fits using the two signal fraction estimations is assigned as an additional uncertainty. The background model uncertainty is estimated by changing the background description using a different nonparameterised method to model the two-body invariant masses and helicity angles considering correlations between them. The variation in the fit results is considered as the systematic uncertainty. The efficiency map category accounts for uncertainties related to the size of the simulation sample used to describe the efficiency variation over the phase space, as well as uncertainties due to simulation corrections. The fixed parameters in the amplitude models include the Blatt-Weisskopf radius parameter and the $f_0(980)$ and $f_2(1270)$ masses and widths. The former is varied from its default value of 3.0 to 1.5 and 4.5 GeV^{-1} . The latter are varied within the uncertainties of previous measurements [16,51]. Additionally, the effect of allowing the γ_2 parameter of the K -matrix $T_{c\bar{s}}$ model to vary in the fit is assigned as a systematic uncertainty.

Possible biases in the fit procedure are studied with pseudoexperiments generated from the fit results, and then fitted with the same model. The pull distribution for each fit parameter is modelled using a Gaussian function for symmetric distributions or a double-sided Crystal Ball function [67] for asymmetric ones. Almost all pull distributions show deviations from normal distributions that are smaller than 3σ . Nonetheless, adjustments are applied to the central values and uncertainties to correct for any potential biases and under- or over-coverage.

For the final results on the mass and width of the $T_{c\bar{s}}$ states, additional systematic uncertainty is assigned to account for the description of the $T_{c\bar{s}}$ lineshape. The results with the $f_0(500) + K\text{-matrix } T_{c\bar{s}}(0^+)$ model are taken as the central values, and an additional asymmetric systematic uncertainty calculated as the difference in the results between the

$f_0(500) + \text{RBW } T_{c\bar{s}}(0^+)$ and $f_0(500) + K\text{-matrix } T_{c\bar{s}}(0^+)$ models is assigned. This is the dominant uncertainty on the $T_{c\bar{s}}$ width. The results for the $T_{c\bar{s}}$ mass and width are $(2327 \pm 13 \pm 13) \text{ MeV}$ and $(96 \pm 16_{-23}^{+170}) \text{ MeV}$, respectively.

8. Summary

An amplitude analysis to study the resonant structure of $D_{s1}(2460)^+ \rightarrow D_s^+ \pi^+ \pi^-$ decays is performed for the first time. The analysis is based on exclusively reconstructed $B^0 \rightarrow D^- D_{s1}(2460)^+$, $B^+ \rightarrow \bar{D}^0 D_{s1}(2460)^+$, and $B^0 \rightarrow D^{*-} D_{s1}(2460)^+$ decays obtained from a pp collision sample recorded at centre-of-mass energies of $\sqrt{s} = 7, 8$ and 13 TeV , corresponding to 9 fb^{-1} of integrated luminosity.

A clear double-peak structure is observed in the $m(\pi^+ \pi^-)$ spectrum of $D_{s1}(2460)^+ \rightarrow D_s^+ \pi^+ \pi^-$ decays. The data can be described well with a model including only $\pi\pi$ resonances and without $D_s^+ \pi$ exotic states, but only with implausibly large $f_0(980)$ and $f_2(1270)$ contributions. In addition, this model has large interference between the $f_0(500)$ and $f_0(980)$ states, which is not seen in other processes involving these two contributions in the $\pi\pi$ S-wave.

An alternative model with a new exotic $T_{c\bar{s}}^{++}$ state and its isospin partner $T_{c\bar{s}}^0$ is introduced. The $T_{c\bar{s}}$ mass and width are determined to be $(2327 \pm 13 \pm 13) \text{ MeV}$ and $(96 \pm 16_{-23}^{+170}) \text{ MeV}$, where the first uncertainties are statistical and the second are systematic. The significance of the new states exceeds 10σ , evaluated relative to a model containing $f_0(500)$ and $f_0(980)$ contributions only, and the $T_{c\bar{s}}$ spin-parity is found to be $J^P = 0^+$ with a significance of 10σ . The $T_{c\bar{s}}$ states can be interpreted as two members of the isotriplet predicted in Ref. [27], with the masses consistent with their prediction. These results complement those obtained on other $T_{c\bar{s}}$ and $T_{c\bar{c}}$ hadrons [20–23], and are an important step to probe the nature of the $D_{s1}(2460)^+$ and $D_{s0}^*(2317)^+$ resonances.

Conflict of interest

The authors declare that they have no conflict of interest.

Acknowledgments

We acknowledge important input from Alex Bondar, which helped to shape the analysis reported here. We express our gratitude to our colleagues in the CERN accelerator departments for the excellent performance of the LHC. We thank the technical and administrative staff at the LHCb institutes. We acknowledge support from CERN and from the national agencies: CAPES, CNPq, FAPERJ and FINEP (Brazil); MOST and NSFC (China); CNRS/IN2P3 (France); BMBF, DFG and MPG (Germany); INFN (Italy); NWO (Netherlands); MNiSW and NCN (Poland); MCID/IFA (Romania); MICIU and AEI (Spain); SNSF and SER (Switzerland); NASU (Ukraine); STFC (United Kingdom); DOE NP and NSF (USA). We acknowledge the computing resources that are provided by CERN, IN2P3 (France), KIT and DESY (Germany), INFN (Italy), SURF (Netherlands), PIC (Spain), GridPP (United Kingdom), CSCS (Switzerland), IFIN-HH (Romania), CBPF (Brazil), and Polish WLCG (Poland). We are indebted to the communities behind the multiple open-source software packages on which we depend. Individual groups or members have received support from ARC and ARDC (Australia); Key Research Program of Frontier Sciences of CAS, CAS PIFI, CAS CCEPP, Fundamental Research Funds for the Central Universities, and Sci. & Tech. Program of Guangzhou (China); Min-ciencias (Colombia); EPLANET, Marie Skłodowska-Curie Actions, ERC and NextGenerationEU (European Union); A*MIDEX, ANR,

IPhU and Labex P2IO, and Région Auvergne-Rhône-Alpes (France); AvH Foundation (Germany); ICSC (Italy); Severo Ochoa and María de Maeztu Units of Excellence, GVA, XuntaGal, GENCAT, InTalent-Inditex and Prog. Atracción Talento CM (Spain); SRC (Sweden); the Leverhulme Trust, the Royal Society and UKRI (United Kingdom).

Appendix A. Supplementary material

Supplementary data to this article can be found online at <https://doi.org/10.1016/j.scib.2025.02.025>.

References

- [1] BaBar Collaboration, Aubert B, et al. Observation of a narrow meson decaying to $D_s^+ \pi^0$ at a mass of $2.32 \text{ GeV}/c^2$. *Phys Rev Lett* 2003;90:242001.
- [2] CLEO Collaboration, Besson D, et al. Observation of a narrow resonance of mass $2.46 \text{ GeV}/c^2$ decaying to $D_s^+ \pi^0$ and confirmation of the $D_{sj}^*(2317)$ state. *Phys Rev D* 2003;68:032002 [Erratum *Phys Rev D* 2007;75:119908].
- [3] Chen YQ, Li XQ. A comprehensive four-quark interpretation of $D_s(2317)$, $D_s(2457)$ and $D_s(2632)$. *Phys Rev Lett* 2004;93:232001.
- [4] Guo FK, Shen PN, Chiang H-C. Dynamically generated 1^+ heavy mesons. *Phys Lett* 2007;B647:133.
- [5] Lutz MFM, Soyeur M. Radiative and isospin-violating decays of D_s mesons in the hadrogenesis conjecture. *Nucl Phys* 2008;A813:14.
- [6] Rosner JL. Effects of S-wave thresholds. *Phys Rev D* 2006;74:076006.
- [7] Feng G-Q, Guo X-H, Zhang Z-H. Studying the D^*K molecular structure of $D_s(2460)$ in the Bethe-Salpeter approach. *Eur Phys J* 2012;C72:2033.
- [8] Ortega PG, Segovia J, Entem DR, et al. Molecular components in P-wave charmed-strange mesons. *Phys Rev D* 2016;94:074037.
- [9] Zhang D, Zhao Q-Y, Zhang Q-Y. A study of S-wave DK interactions in the chiral $SU(3)$ quark model. *Chin Phys Lett* 2009;26:091201.
- [10] Mehen T, Springer RP. Heavy-quark symmetry and the electromagnetic decays of excited charmed strange mesons. *Phys Rev D* 2004;70:074014.
- [11] Belle Collaboration, Choi S-K, et al. Measurements of $B \rightarrow \bar{D}D_{s0}^+(2317)$ decay rates and a search for isospin partners of the $D_{s0}^+(2317)$. *Phys Rev D* 2015;91:092011 [Erratum *Phys Rev D* 2015;92:039905].
- [12] Hadron Spectrum Collaboration, Yeo JDE, et al. $DK/D\pi$ scattering and an exotic virtual bound state at the $SU(3)$ flavour symmetric point from lattice QCD. *J High Energy Phys* 2024;07:012.
- [13] Godfrey S, Isgur N. Mesons in a relativized quark model with chromodynamics. *Phys Rev D* 1985;32:189.
- [14] Godfrey S, Kokoski R. Properties of P-wave mesons with one heavy quark. *Phys Rev D* 1991;43:1679.
- [15] Di Pierro M, Eichten E. Excited heavy-light systems and hadronic transitions. *Phys Rev D* 2001;64:114004.
- [16] Group Particle Data, Navas S, et al. Review of particle physics. *Phys Rev D* 2024;110:030001.
- [17] BaBar Collaboration, Aubert B, et al. A study of the $D_{sj}^*(2317)^+$ and $D_{sj}(2460)^+$ mesons in inclusive $c\bar{c}$ production near $\sqrt{s} = 10.6 \text{ GeV}$. *Phys Rev D* 2006;74:032007.
- [18] Belle Collaboration, Mikami Y, et al. Measurements of the D_{sj} resonance properties. *Phys Rev Lett* 2004;92:012002.
- [19] Tang M-N, Lin Y-H, Guo F-K, et al. Isospin-conserving hadronic decay of the $D_{s1}(2460)$ into $D_s \pi^+ \pi^-$. *Commun Theor Phys* 2023;75:055203.
- [20] LHCb Collaboration, Aaij R, et al. Model-independent study of structure in $B^+ \rightarrow D^+ D^- K^+$ decays. *Phys Rev Lett* 2020;125:242001.
- [21] LHCb Collaboration, Aaij R, et al. Amplitude analysis of the $B^+ \rightarrow D^+ D^- K^+$ decay. *Phys Rev D* 2020;102:112003.
- [22] LHCb Collaboration, Aaij R, et al. First observation of a doubly charged tetraquark candidate and its neutral partner. *Phys Rev Lett* 2023;131:041902.
- [23] LHCb Collaboration, Aaij R, et al. Amplitude analysis of $B^0 \rightarrow \bar{D}^0 D_s^+ \pi^-$ and $B^+ \rightarrow D^- D_s^+ \pi^+$ decays. *Phys Rev D* 2023;108:012017.
- [24] Ke H-W, Shi Y-F, Liu X-H, et al. Possible molecular states of $\bar{D}^* K^*$ ($D^* K^*$) and new exotic states $X_0(2900)$, $X_1(2900)$, $T_{cs0}(2900)^0$ and $T_{cs0}^+(2900)^{++}$. *Phys Rev D* 2022;106:114032.
- [25] Agaev SS, Azizi K, Sundu H. Modeling the resonance $T_{cs0}^+(2900)^{++}$ as a hadronic molecule $D^+ K^{*+}$. *Phys Rev D* 2023;107:094019.
- [26] Duan M-Y, Du M-L, Guo Z-H, et al. Coupled-channel $D^* K^* - D_s^* \rho$ interactions and the origin of $T_{cs0}(2900)$. *Phys Rev D* 2023;108:074006.
- [27] Maiani L, Polosa A D, Riquer V. Open charm tetraquarks in broken $SU(3)_F$ symmetry. *Phys Rev D* 2024;110:034014.
- [28] Terasaki K. BABAR resonance as a new window of hadron physics. *Phys Rev D* 2003;68:011501.
- [29] LHCb Collaboration, Alves Jr AA, et al. The LHCb detector at the LHC. *J Instrum* 2008;3:S08005.
- [30] LHCb Collaboration, Aaij R, et al. LHCb detector performance. *Int J Mod Phys* 2015;A30:1530022.
- [31] Sjöstrand T, Mrenna S, Skands P. A brief introduction to PYTHIA 8.1. *Comput Phys Commun* 2008;178:852.
- [32] Sjöstrand T, Mrenna S, Skands P. PYTHIA 6.4 physics and manual. *J High Energy Phys* 2006;05:026.
- [33] Belyaev I, Brambach T, H Brook N, et al. Handling of the generation of primary events in Gauss, the LHCb simulation framework. *J Phys Conf Ser* 2011;331:032047.
- [34] Lange DJ. The EvtGen particle decay simulation package. *Nucl Instrum Meth* 2001;A462:152.
- [35] Davidson N, Przedzinski T, Was Z. PHOTOS interface in C++: technical and physics documentation. *Comp Phys Comm* 2016;199:86.
- [36] Geant4 Collaboration, Allison J, et al. Geant4 developments and applications. *IEEE Trans Nucl Sci* 2006;53:270.
- [37] Geant4 Collaboration, Agostinelli S, et al. Geant4: a simulation toolkit. *Nucl Instrum Meth* 2003;A506:250.
- [38] Clemencic M, Corti G, Easo S, et al. The LHCb simulation application, Gauss: design, evolution and experience. *J Phys Conf Ser* 2011;331:032023.
- [39] Müller D, Clemencic M, Corti G, et al. ReDecay: a novel approach to speed up the simulation at LHCb. *Eur Phys J* 2018;C78:1009.
- [40] Breiman L, H Friedman J, A Olshen R, et al. Classification and Regression Trees. Belmont: Wadsworth International Group; 1984.
- [41] Freund Y, Schapire RE. A decision-theoretic generalization of on-line learning and an application to boosting. *J Comput Syst Sci* 1997;55:119.
- [42] Voss H, Hoecker A, Stelzer J, et al. TMVA-Toolkit for multivariate data analysis with ROOT. In: Proceedings of the XI international workshop on advanced computing and analysis techniques in physics research (ACAT) 2007.
- [43] Hoecker A, Speckmayer P, Stelzer J, et al. TMVA 4—Toolkit for Multivariate data analysis with ROOT. Users guide 2007. arXiv:physics/0703039.
- [44] Hulsbergen WD. Decay chain fitting with a Kalman filter. *Nucl Instrum Meth* 2005;A552:566.
- [45] ARGUS Collaboration, Albrecht H, et al. Search for hadronic $b \rightarrow u$ decays. *Phys Lett B* 1990;B241:278.
- [46] Fleming GN. Recoupling effects in the isobar model. I. General formalism for three-pion scattering. *Phys Rev* 1964;135:B551.
- [47] Morgan D. Phenomenological analysis of $I = \frac{1}{2}$ single-pion production processes in the energy range 500 to 700 MeV. *Phys Rev* 1968;166:1731.
- [48] Herndon DJ, Söding P, Cashmore RJ. Generalized isobar model formalism. *Phys Rev* 1975;D11:3165.
- [49] Flatté SM. Coupled-channel analysis of the $\pi\eta$ and $K\bar{K}$ systems near $K\bar{K}$ threshold. *Phys Lett B* 1976;63:224.
- [50] Bugg DV. Reanalysis of data on $a_0(1450)$ and $a_0(980)$. *Phys Rev D* 2008;78:074023.
- [51] LHCb Collaboration, Aaij R, et al. Measurement of resonant and CP components in $\bar{B}_s^0 \rightarrow J/\psi \pi^+ \pi^-$ decays. *Phys Rev D* 2014;D89:092006.
- [52] Aitchison IJR. K-matrix formalism for overlapping resonances. *Nucl Phys* 1972;A189:417.
- [53] Anisovich VV, Sarantsev AV. K matrix analysis of the ($J^{PC} = 0^{++}$)-wave in the mass region below 1900 MeV. *Eur Phys J* 2003;A16:229.
- [54] JPAC Collaboration, Fernández-Ramírez C, et al. Interpretation of the LHCb $P_c(4312)^+$ signal. *Phys Rev Lett* 2019;123:092001.
- [55] LHCb Collaboration, Aaij R, et al. Measurement of the track reconstruction efficiency at LHCb. *J Instrument* 2015;10:P02007.
- [56] Aaij R, Albrecht J, Alessio F, et al. The LHCb trigger and its performance in 2011. *J Instrument* 2013;8:P04022.
- [57] Poluektov A. Kernel density estimation of a multidimensional efficiency profile. *J Instrument* 2015;10:P02011.
- [58] LHCb Collaboration, Aaij R, et al. Measurement of the resonant and CP components in $\bar{B}^0 \rightarrow J/\psi \pi^+ \pi^-$ decays. *Phys Rev D* 2014;90:012003.
- [59] LHCb Collaboration, Aaij R, et al. Dalitz plot analysis of $B^0 \rightarrow \bar{D}^0 \pi^+ \pi^-$ decays. *Phys Rev D* 2015;92:032002.
- [60] LHCb Collaboration, Aaij R, et al. Amplitude analysis of the $B^+ \rightarrow \pi^+ \pi^+ \pi^-$ decay. *Phys Rev D* 2020;101:012006.
- [61] LHCb Collaboration, Aaij R, et al. Amplitude analysis of the $D^+ \rightarrow \pi^- \pi^+ \pi^+$ decay and measurement of the $\pi^- \pi^+$ S-wave amplitude. *J High Energy Phys* 2023;06:044.
- [62] LHCb Collaboration, Aaij R, et al. Amplitude analysis of the $D_s^+ \rightarrow \pi^- \pi^+ \pi^+$ decay. *J High Energy Phys* 2023;07:204.
- [63] BES Collaboration, Ablikim M, et al. Resonances in $J/\psi \rightarrow \phi \pi^+ \pi^-$ and $\phi K^+ K^-$. *Phys Lett B* 2005;607:243.
- [64] BESIII Collaboration, Ablikim M, et al. Amplitude analysis of the decays $\eta' \rightarrow \pi^+ \pi^- \pi^0$ and $\eta' \rightarrow \pi^0 \pi^0 \pi^0$. *Phys Rev Lett* 2017;118:012001.
- [65] Liu L, Orginos K, Guo F-K, et al. Interactions of charmed mesons with light pseudoscalar mesons from lattice QCD and implications on the nature of the $D_{s0}^*(2317)$. *Phys Rev D* 2013;87:014508.
- [66] Guo F-K, Hanhart C, Meissner U-G. Interactions between heavy mesons and Goldstone bosons from chiral dynamics. *Eur Phys J* 2009;A40:171.
- [67] Skwarnicki TA. Study of the radiative cascade transitions between the upsilon-prime and upsilon resonances. Dissertation for doctoral degree. Krakow: Institute of Nuclear Physics; 1986.

LHCb collaboration

R. Aaij³⁸, A.S.W. Abdelmotteleb⁵⁷, C.Abellan Beteta⁵¹, F. Abudinén⁵⁷, T. Ackernley⁶¹, A.A. Adefisoye⁶⁹, B. Adeva⁴⁷, M. Adinolfi⁵⁵, P. Adlarson⁸², C. Agapopoulou¹⁴, C.A. Aidala⁸³, Z. Ajaltouni¹¹, S. Akar⁶⁶, K. Akiba³⁸, P. Albicocco²⁸, J. Albrecht¹⁹, F. Alessio⁴⁹, M. Alexander⁶⁰, Z. Aliouche⁶³, P.Alvarez Cartelle⁵⁶, R. Amalric¹⁶, S. Amato³, J.L. Amey⁵⁵, Y. Amhis¹⁴, L. An⁶, L. Anderlini²⁷, M. Andersson⁵¹, A. Andreianov⁴⁴, P. Andreola⁵¹, M. Andreotti²⁶, D. Andreou⁶⁹, A. Anelli^{31,n}, D. Ao⁷, F. Archilli^{37,t}, M. Argenton²⁶, S.Argueda Cuendis^{9,49}, A. Artamonov⁴⁴, M. Artuso⁶⁹, E. Aslanides¹³, R.Ataíde Da Silva⁵⁰, M. Atzeni⁶⁵, B. Audurier¹², D. Bacher⁶⁴, I.Bachiller Perea¹⁰, S. Bachmann²², M. Bachmayer⁵⁰, J.J. Back⁵⁷, P.Baladron Rodriguez⁴⁷, V. Balagura¹⁵, A. Balboni²⁶, W. Baldini²⁶, L. Balzani¹⁹, H. Bao⁷, J.Baptista de Souza Leite⁶¹, C.Barbero Pretel⁴⁷, M. Barbetti²⁷, I.R. Barbosa⁷⁰, R.J. Barlow⁶³, M. Barnyakov²⁵, S. Barsuk¹⁴, W. Barter⁵⁹, M. Bartolini⁵⁶, J. Bartz⁶⁹, J.M. Basels¹⁷, S. Bashir⁴⁰, G. Bassi¹⁹, B. Batsukh⁵, P.B. Battista¹⁴, A. Bay⁵⁰, A. Beck⁵⁷, M. Becker¹⁹, F. Bedeschi³⁵, I.B. Bediaga², N.B. Behling¹⁹, S. Belin⁴⁷, K. Belov⁴⁴, I. Belov²⁹, I. Belyaev³⁶, G. Benane¹³, G. Bencivenni²⁸, E. Ben-Haim¹⁶, A. Berezhniov⁴⁴, R. Bernet⁵¹, S.Bernet Andres⁴⁵, A. Bertolin³³, C. Betancourt⁵¹, F. Betti⁵⁹, J. Bex⁵⁶, Ia. Bezshyiko⁵¹, J. Bhom⁴¹, M.S. Bieker¹⁹, N.V. Biesuz²⁶, P. Billoir¹⁶, A. Biolchini³⁸, M. Birch⁶², F.C.R. Bishop¹⁰, A. Bitadze⁶³, A. Bizzeti, T. Blake⁵⁷, F. Blanc⁵⁰, J.E. Blank¹⁹, S. Blusk⁶⁹, V. Bocharnikov⁴⁴, J.A. Boelhaue¹⁹, O.Boente Garcia¹⁵, T. Boettcher⁶⁶, A. Bohare⁵⁹, A. Boldyrev⁴⁴, C.S. Bolognani⁷⁹, R. Bolzonella^{26,k}, R.B. Bonacci¹, N. Bondar⁴⁴, A. Bordellius⁴⁹, F. Borgato^{33,o}, S. Borghi⁶³, M. Borsato^{31,n}, J.T. Borsuk⁴¹, S.A. Bouchiba⁵⁰, M. Bovill⁶⁴, T.J.V. Bowcock⁶¹, A. Boyer⁴⁹, C. Bozzi²⁶, A.Brea Rodriguez⁵⁰, N. Breer¹⁹, J. Brodzicka⁴¹, A.Brossa Gonzalo^{47,†}, J. Brown⁶¹, D. Brundu³², E. Buchanan⁵⁹, A. Buonauro⁵¹, L. Buonincontri^{33,o}, A.T. Burke⁶³, C. Burr⁴⁹, J.S. Butter⁵⁶, J. Buytaert⁴⁹, W. Byczynski⁴⁹, S. Cadeddu³², H. Cai⁷⁴, A.C. Caillet¹⁶, R. Calabrese^{26,k}, S.Calderon Ramirez⁹, L. Calefice⁴⁶, S. Cali²⁸, M. Calvi^{31,n}, M.Calvo Gomez⁴⁵, P.Camargo Magalhaes^{2,x}, J.I. Cambon Bouzas⁴⁷, P. Campana²⁸, D.H.Campora Perez⁷⁹, A.F.Campoverde Quezada⁷, S. Capelli³¹, L. Capriotti²⁶, R. Caravaca-Mora⁹, A. Carbone^{25,i}, L.Carcedo Salgado⁴⁷, R. Cardinale^{29,i}, A. Cardini³², P. Carniti^{31,n}, L. Carus²², A.Casais Vidal⁶⁵, R. Caspary²², G. Casse⁶¹, M. Cattaneo⁴⁹, G. Cavallero^{26,49}, V. Cavallini^{26,k}, S. Celani²², D. Cervenkov⁶⁴, S. Cesare^{30,m}, A.J. Chadwick⁶¹, I. Chahrouh⁸³, M. Charles¹⁶, Ph. Charpentier⁴⁹, E. Chatzianagnostou³⁸, M. Chefdeville¹⁰, C. Chen¹³, S. Chen⁵, Z. Chen⁷, A. Chernov⁴¹, S. Chernyshenko⁵³, X. Chiotopoulos⁷⁹, V. Chobanova⁸¹, S. Cholak⁵⁰, M. Chruszcz⁴¹, A. Chubykin⁴⁴, V. Chulikov²⁸, P. Ciambriano²⁸, X.Cid Vidal⁴⁷, G. Ciezarek⁴⁹, P. Cifra⁴⁹, P.E.L. Clarke⁵⁹, M. Clemencic⁴⁹, H.V. Cliff⁵⁶, J. Closier⁴⁹, C.Cocha Toapaxi²², V. Coco⁴⁹, J. Cogan¹³, E. Cogneras¹¹, L. Cojocariu⁴³, S. Collaviti⁵⁰, P. Collins⁴⁹, T. Colombo⁴⁹, M.C. Colonna¹⁹, A. Comerma-Montells⁴⁶, L. Congedo²⁴, A. Contu³², N. Cooke⁶⁰, I. Corredoira⁴⁷, A. Correia¹⁶, G. Corti⁴⁹, J.J.Cottee Meldrum⁵⁵, B. Couturier⁴⁹, D.C. Craik⁵¹, M.Cruz Torres^{2,f}, E.Curras Rivera⁵⁰, R. Currie⁵⁹, C.L.Da Silva⁶⁸, S. Dadabaev⁴⁴, L. Dai⁷¹, X. Dai⁶, E. Dall'Occo⁴⁹, J. Dalseno⁴⁷, C. D'Ambrosio⁴⁹, J. Daniel¹¹, A. Danilina⁴⁴, P. d'Argent²⁴, A. Davidson⁵⁷, J.E. Davies⁶³, A. Davis⁶³, O.De Aguiar Francisco⁶³, C.De Angelis^{32,j}, F.De Benedetti⁴⁹, J. de Boer³⁸, K.De Bruyn⁷⁸, S.De Capua⁶³, M.De Cian²², U.De Freitas Carneiro Da Graca^{2,a}, E.De Lucia²⁸, J.M.De Miranda², L.De Paula³, M.De Serio^{24,g}, P.De Simone²⁸, F.De Vellis¹⁹, J.A. de Vries⁷⁹, F. Debernardis²⁴, D. Decamp¹⁰, V. Dedu¹³, S. Dekkers¹, L.Del Buono¹⁶, B. Delaney⁶⁵, H.-P. Dembinski¹⁹, J. Deng⁸, V. Denysenko⁵¹, O. Deschamps¹¹, F. Dettori^{32,j}, B. Dey⁷⁷, P.Di Nezza²⁸, I. Diachkov⁴⁴, S. Didenko⁴⁴, S. Ding⁶⁹, L. Dittmann²², V. Dobishuk⁵³, A.D. Docheva⁶⁰, C. Dong^{4,b}, A.M. Donohoe²³, F. Dordei³², A.C. dos Reis², A.D. Dowling⁶⁹, W. Duan⁷², P. Duda⁸⁰, M.W. Dudek⁴¹, L. Dufour⁴⁹, V. Duk³⁴, P. Durante⁴⁹, M.M. Duras⁸⁰, J.M. Durham⁶⁸, O.D. Durmus⁷⁷, A. Dziurda⁴¹, A. Dzyuba⁴⁴, S. Easo⁵⁸, E. Eckstein¹⁸, U. Egede¹, A. Egorychev⁴⁴, V. Egorychev⁴⁴, S. Eisenhardt⁵⁹, E. Ejopu⁶³, L. Eklund⁸², M. Elashri⁶⁶, J. Ellbracht¹⁹, S. Ely⁶², A. Ene⁴³, J. Eschle⁶⁹, S. Esen²², T. Evans⁶³, F. Fabiano^{32,j}, L.N. Falcao², Y. Fan⁷, B. Fang⁷, L. Fantini^{34,p,49}, M. Faria⁵⁰, K. Farmer⁵⁹, D. Fazzini^{31,n}, L. Felkowski⁸⁰, M. Feng^{5,7}, M. Feo¹⁹, A.Fernandez Casani⁴⁸, M.Fernandez Gomez⁴⁷, A.D. Fernez⁶⁷, F. Ferrari²⁵, F.Ferreira Rodrigues³, M. Ferrillo⁵¹, M. Ferro-Luzzi⁴⁹, S. Filippov⁴⁴, R.A. Fini²⁴, M. Fiorini^{26,k}, M. Firlje⁴⁰, K.L. Fischer⁶⁴, D.S. Fitzgerald⁸³, C. Fitzpatrick⁶³, T. Fiutowski⁴⁰, F. Fleuret¹⁵, M. Fontana²⁵, L.F. Foreman⁶³, R. Forty⁴⁹, D. Foulds-Holt⁵⁶, V.Franco Lima³, M.Franco Sevilla⁶⁷, M. Frank⁴⁹, E. Franzoso^{26,k}, G. Frau⁶³, C. Frei⁴⁹, D.A. Friday⁶³, J. Fu⁷, Q. Fuehring^{19,56}, Y. Fujii¹, T. Fulghesu¹⁶, E. Gabriel³⁸, G. Galati²⁴, M.D. Galati³⁸, A.Gallas Torreira⁴⁷, D. Galli^{25,i}, S. Gambetta⁵⁹, M. Gandelman³, P. Gandini³⁰, B. Ganie⁶³, H. Gao⁷, R. Gao⁶⁴, T.Q. Gao⁵⁶, Y. Gao⁸, Y. Gao⁶, Y. Gao⁸, L.M.Garcia Martin⁵⁰, P.Garcia Moreno⁴⁶, J.Garca Pardiñas⁴⁹, P. Gardner⁶⁷, K.G. Garg⁸, L. Garrido⁴⁶, C. Gaspar⁴⁹, R.E. Geertsema³⁸, L.L. Gerken¹⁹, E. Gersabeck⁶³, M. Gersabeck²⁰, T. Gershon⁵⁷, S.G. Ghizzo²⁹, Z. Ghorbanimoghaddam⁵⁵, L. Giambastiani^{33,o}, F.I. Giasemis^{16,e}, V. Gibson⁵⁶, H.K. Gienza⁴², A.L. Gilman⁶⁴, M. Giovannetti²⁸, A. Gioventù⁴⁶, L. Girardey⁶³, P.Gironella Gironell⁴⁶, C. Giugliano^{26,k}, M.A. Giza⁴¹, E.L. Gkougkousis⁶², F.C. Glaser^{14,22}, V.V. Gligorov^{16,49}, C. Göbel⁷⁰, E. Golobardes⁴⁵, D. Golubkov⁴⁴, A. Golutvin^{62,44,49}, S.Gomez Fernandez⁴⁶, W. Gomulka⁴⁰, F.Goncalves Abrantes⁶⁴, M. Goncerz⁴¹, G. Gong^{4,b}, J.A. Gooding¹⁹, I.V. Gorelov⁴⁴, C. Gotti³¹, J.P. Grabowski¹⁸, L.A.Granado Cardoso⁴⁹, E. Graugés⁴⁶, E. Graverini^{50,r}, L. Grazette⁵⁷, G. Graziani, A.T. Grecu⁴³, L.M. Greeven³⁸, N.A. Grieser⁶⁶, L. Grillo⁶⁰, S. Gromov⁴⁴, C. Gu¹⁵, M. Guarise²⁶, L. Guerry¹¹, M. Guittiere¹⁴, V. Guliaeva⁴⁴, P.A. Günther²², A.-K. Guseinov⁵⁰, E. Gushchin⁴⁴, Y. Guz^{6,44,49}, T. Gys⁴⁹, K. Habermann¹⁸, T. Hadavizadeh¹, C. Hadjivasiliou⁶⁷, G. Haefeli⁵⁰, C. Haen⁴⁹, M. Hajheidari⁴⁹, G.H. Hallett⁵⁷, M.M. Halvorsen⁴⁹, P.M. Hamilton⁶⁷, J. Hammerich⁶¹, Q. Han⁸, X. Han^{22,49}, S. Hansmann-Menzemer²², L. Hao⁷, N. Harnew⁶⁴, T.H. Harris¹, M. Hartmann¹⁴, S. Hashmi⁴⁰, J. He^{7,c}, F. Henner⁴⁹, C. Henderson⁶⁶, R.D.L. Henderson^{1,57}, A.M. Hennequin⁴⁹, K. Hennessy⁶¹, L. Henry⁵⁰, J. Herd⁶², P.Herrero Gascon²², J. Heuel¹⁷, A. Hicheur³, G.Hijano Mendizabal⁵¹, J. Horswill⁶³, R. Hou⁸, Y. Hou¹¹, N. Howarth⁶¹, J. Hu⁷², W. Hu⁶, X. Hu^{4,b}, W. Huang⁷, W. Hulsbergen³⁸, R.J. Hunter⁵⁷, M. Hushchyn⁴⁴, D. Hutchcroft⁶¹, M. Idzik⁴⁰, D. Ilin⁴⁴, P. Ilten⁶⁶, A. Inglessi⁴⁴, A. Iniuukhin⁴⁴, A. Ishteev⁴⁴, K. Ivshin⁴⁴, R. Jacobsson⁴⁹, H. Jage¹⁷, S.J.Jaimes Elles^{75,49,48}, S. Jakobsen⁴⁹, E. Jans³⁸, B.K. Jashal⁴⁸, A. Jawahery^{67,49}, V. Jevtic¹⁹, E. Jiang⁶⁷, X. Jiang^{5,7}, Y. Jiang⁷, Y.J. Jiang⁶, M. John⁶⁴, A.John Rubesh Rajan²³, D. Johnson⁵⁴, C.R. Jones⁵⁶, T.P. Jones⁵⁷, S. Joshi⁴², B. Jost⁴⁹, J.Juan Castella⁵⁶, N. Jurik⁴⁹, I. Juszcak⁴¹, D. Kaminaris⁵⁰, S. Kandybei⁵², M. Kane⁵⁹, Y. Kang^{4,b}, C. Kar¹¹, M. Karacson⁴⁹, D. Karpenkov⁴⁴, A. Kauniskangas⁵⁰, J.W. Kautz⁶⁶, M.K. Kazanecki⁴¹, F. Keizer⁴⁹, M. Kenzie⁵⁶, T. Ketel³⁸, B. Khanji⁶⁹, A. Kharisova⁴⁴, S. Kholodenko^{35,49}, G. Khreich¹⁴, T. Kirn¹⁷, V.S. Kirsebom^{31,n}, O. Kitouni⁶⁵, S. Klaver³⁹, N. Klejne^{35,q}, K. Klimaszewski⁴², M.R. Kmiec⁴², S. Koliiev⁵³, L. Kolk¹⁹, A. Konoplyannikov⁴⁴, P. Kopciwicz^{40,49}, P. Koppenburg³⁸, M. Korolev⁴⁴, I. Kostiuik³⁸, O. Kot⁵³, S. Kotriakhova, A. Kozachuk⁴⁴, P. Kravchenko⁴⁴, L. Kravchuk⁴⁴, M. Kreps⁵⁷, P. Krokovny⁴⁴, W. Krupa⁶⁹, W. Krzemien⁴², O.K. Kshyvanskyi⁵³, S. Kubis⁸⁰, M. Kucharczyk⁴¹, V. Kudryavtsev⁴⁴, E. Kulikova⁴⁴, A. Kupsc⁸², B.K. Kutsenko¹³

D. Lacarrere⁴⁹, P.Laguarta Gonzalez⁴⁶, A. Lai³², A. Lampis³², D. Lancierini⁵⁶, C.Landesa Gomez⁴⁷, J.J. Lane¹, R. Lane⁵⁵, G. Lanfranchi²⁸, C. Langenbruch²², J. Langer¹⁹, O. Lantwin⁴⁴, T. Latham⁵⁷, F. Lazzari^{35,r}, C. Lazzeroni⁵⁴, R.Le Gac¹³, H. Lee⁶¹, R. Lefèvre¹¹, A. Leflat⁴⁴, S. Legotin⁴⁴, M. Lehuraux⁵⁷, E.Lemos Cid⁴⁹, O. Leroy¹³, T. Lesiak⁴¹, E. Lesser⁴⁹, B. Leverington²², A. Li^{4,b}, C. Li¹³, H. Li⁷², K. Li⁸, L. Li⁶³, M. Li⁸, P. Li⁷, P.-R. Li⁷³, Q. Li^{5,7}, S. Li⁸, T. Li^{5,d}, T. Li⁷², Y. Li⁸, Y. Li⁵, Z. Lian^{4,b}, X. Liang⁶⁹, S. Libralon⁴⁸, C. Lin⁷, T. Lin⁵⁸, R. Lindner⁴⁹, H. Linton⁶², V. Lisovskyi⁵⁰, R. Litvinov^{32,49}, F.L. Liu¹, G. Liu⁷², K. Liu⁷³, S. Liu^{5,7}, W. Liu⁸, Y. Liu⁵⁹, Y. Liu⁷³, Y.L. Liu⁶², A.Lobo Salvia⁴⁶, A. Loi³², T. Long⁵⁶, J.H. Lopes³, A.Lopez Huertas⁴⁶, S.López Soliño⁴⁷, Q. Lu¹⁵, C. Lucarelli²⁷, D. Lucchesi^{33,o}, M.Lucio Martinez⁷⁹, V. Lukashenko^{38,53}, Y. Luo⁶, A. Lupato^{33,h}, E. Luppi^{26,k}, K. Lynch²³, X.-R. Lyu⁷, G.M. Ma^{4,b}, S. Maccolini¹⁹, F. Machefert¹⁴, F. Maciuc⁴³, B. Mack⁶⁹, I. Mackay⁶⁴, L.M. Mackey⁶⁹, L.R.Madhan Mohan⁵⁶, M.J. Madurai⁵⁴, A. Maevskiy⁴⁴, D. Magdalinski³⁸, D. Maisuzenko⁴⁴, M.W. Majewski⁴⁰, J.J. Malczewski⁴¹, S. Malde⁶⁴, L. Malentacca⁴⁹, A. Malinin⁴⁴, R. Manera Escalero⁴⁶, F.M. Mangano³⁷, D. Manuzzi²⁵, D. Marangotto^{30,m}, J.F. Marchand¹⁰, R. Marchevski⁵⁰, U. Marconi²⁵, E. Mariani¹⁶, S. Mariani⁴⁹, C.Marin Benito^{46,49}, J. Marks²², A.M. Marshall⁵⁵, L. Martel⁶⁴, G. Martelli^{34,p}, G. Martellotti³⁶, L. Martinazzoli⁴⁹, M. Martinelli^{31,n}, D.Martinez Gomez⁷⁸, D.Martinez Santos⁸¹, F.Martinez Vidal⁴⁸, A.Martorell i Granollers⁴⁵, A. Massafferri², R. Matev⁴⁹, A. Mathad⁴⁹, V. Matiunin⁴⁴, C. Matteuzzi⁶⁹, K.R. Mattioli¹⁵, A. Mauri⁶², E. Maurice¹⁵, J. Mauricio⁴⁶, P. Mayencourt⁵⁰, J.Mazorra de Cos⁴⁸, M. Mazurek⁴², M. McCann⁶², L. Mcconnell²³, T.H. McGrath⁶³, N.T. McHugh⁶⁰, A. McNab⁶³, R. McNulty²³, B. Meadows⁶⁶, G. Meier¹⁹, D. Melnychuk⁴², F.M. Meng^{4,b}, M. Merk^{38,79}, A. Merli⁵⁰, L.Meyer Garcia⁶⁷, D. Miao^{5,7}, H. Miao⁷, M. Mikhasenko⁷⁶, D.A. Milanes⁷⁵, A. Minotti^{31,n}, E. Minucci²⁸, T. Miralles¹¹, B. Mitreska¹⁹, D.S. Mitzel¹⁹, A. Modak⁵⁸, R.A. Mohammed⁶⁴, R.D. Moise¹⁷, S. Mokhnenko⁴⁴, E.F. Molina Cardenas⁸³, T. Mombächer⁴⁹, M. Monk^{57,1}, S. Monteil¹¹, A.Morcillo Gomez⁴⁷, G. Morello²⁸, M.J. Morello^{35,q}, M.P. Morgenthaler²², J. Moron⁴⁰, W. Morren³⁸, A.B. Morris⁴⁹, A.G. Morris¹³, R. Mountain⁶⁹, H. Mu^{4,b}, Z.M. Mu⁶, E. Muhammad⁵⁷, F. Muheim⁵⁹, M. Mulder⁷⁸, K. Müller⁵¹, F. Muñoz-Rojas⁹, R. Murta⁶², P. Naik⁶¹, T. Nakada⁵⁰, R. Nandakumar⁵⁸, T. Nanut⁴⁹, I. Nasteva³, M. Needham⁵⁹, N. Neri^{30,m}, S. Neubert¹⁸, N. Neufeld⁴⁹, P. Neustroev⁴⁴, J. Nicolini^{19,14}, D. Nicotra⁷⁹, E.M. Niel⁴⁹, N. Nikitin⁴⁴, P. Nogarolli³, P. Nogga¹⁸, C. Normand⁵⁵, J.Novoa Fernandez⁴⁷, G. Nowak⁶⁶, C. Nunez⁸³, H.N. Nur⁶⁰, A. Oblakowska-Mucha⁴⁰, V. Obraztsov⁴⁴, T. Oeser¹⁷, S. Okamura^{26,k}, A. Okhotnikov⁴⁴, O. Okhrimenko⁵³, R. Oldeman^{32,j}, F. Oliva⁵⁹, M. Olocco¹⁹, C.J.G. Onderwater⁷⁹, R.H. O’Neil⁵⁹, D. Osthues¹⁹, J.M.Otalora Goicochea³, P. Owen⁵¹, A. Oyaguren⁴⁸, O. Ozcelik⁵⁹, F. Paciolla^{35,u}, A. Padee⁴², K.O. Padeken¹⁸, B. Pagare⁵⁷, P.R. Pais²², T. Pajero⁴⁹, A. Palano²⁴, M. Palutan²⁸, X. Pan^{4,b}, G. Panshin⁴⁴, L. Paolucci⁵⁷, A. Papanestis^{58,49}, M. Pappagallo^{24,g}, L.L. Pappalardo^{26,k}, C. Pappenheimer⁶⁶, C. Parkes⁶³, D. Parmar⁷⁶, B. Passalacqua^{26,k}, G. Passaleva²⁷, D. Passaro^{35,q}, A. Pastore²⁴, M. Patel⁶², J. Patoc⁶⁴, C. Patrignani^{25,1}, A. Paul⁶⁹, C.J. Pawley⁷⁹, A. Pellegrino³⁸, J. Peng^{5,7}, M.Pepe Altarelli²⁸, S. Perazzini²⁵, D. Pereima⁴⁴, H.Pereira Da Costa⁶⁸, A.Pereiro Castro⁴⁷, P. Perret¹¹, A. Perrevoort⁷⁸, A. Perro⁴⁹, K. Petridis⁵⁵, A. Petrolini^{29,1}, J.P. Pfaller⁶⁶, H. Pham⁶⁹, L. Pica^{35,q}, M. Piccini³⁴, L. Piccolo³², B. Pietrzyk¹⁰, G. Pietrzyk¹⁴, D. Pinci³⁶, F. Pisani⁴⁹, M. Pizzichemi^{31,n}, V. Placinta⁴³, M.Plo Casasus⁴⁷, T. Poeschl⁴⁹, F. Polci^{16,49}, M.Poli Lener²⁸, A. Poluektov¹³, N. Polukhina⁴⁴, I. Polyakov⁴⁴, E. Polycarpo³, S. Ponce⁴⁹, D. Popov⁷, S. Poslavskii⁴⁴, K. Prasanth⁵⁹, C. Prouve⁸¹, D. Provenzano^{32,j}, V. Pugatch⁵³, G. Punzi^{35,r}, S. Qasim⁵¹, Q.Q. Qian⁶, W. Qian⁷, N. Qin^{4,b}, S. Qu^{4,b}, R. Quagliani⁴⁹, R.I.Rabadan Trejo⁵⁷, J.H. Rademacker⁵⁵, M. Rama³⁵, M.Ramírez García⁸³, V.Ramos De Oliveira⁷⁰, M.Ramos Pernas⁵⁷, M.S. Rangel³, F. Ratnikov⁴⁴, G. Raven³⁹, M.Rebollo De Miguel⁴⁸, F. Redi^{30,h}, J. Reich⁵⁵, F. Reiss⁶³, Z. Ren⁷, P.K. Resmi⁶⁴, R. Ribatti⁵⁰, G.R. Ricart^{15,12}, D. Ricciardi^{35,q}, S. Ricciardi⁵⁸, K. Richardson⁶⁵, M. Richardson-Slipper⁵⁹, K. Rinnert⁶¹, P. Robbe^{14,49}, G. Robertson⁶⁰, E. Rodrigues⁶¹, A.Rodríguez Alvarez⁴⁶, E.Rodríguez Fernandez⁴⁷, J.A.Rodríguez Lopez⁷⁵, E.Rodríguez Rodriguez⁴⁷, J. Roensch¹⁹, A. Rogachev⁴⁴, A. Rogovskiy⁵⁸, D.L. Rolf⁴⁹, P. Roloff⁴⁹, V. Romanovskiy⁶⁶, A.Romero Vidal⁴⁷, G. Romolini²⁶, F. Ronchetti⁵⁰, T. Rong⁶, M. Rotondo²⁸, S.R. Roy²², M.S. Rudolph⁶⁹, M.Ruiz Diaz²², R.A.Ruiz Fernandez⁴⁷, J.Ruiz Vidal^{82,y}, A. Ryzhikov⁴⁴, J. Ryzka⁴⁰, J.J. Saavedra-Arias⁹, J.J.Saborido Silva⁴⁷, R. Sadek¹⁵, N. Sagidova⁴⁴, D. Sahoo⁷⁷, N. Sahoo⁵⁴, B. Saitta^{32,j}, M. Salomoni^{31,n,49}, I. Sanderswood⁴⁸, R. Santacesaria³⁶, C.Santamarina Rios⁴⁷, M. Santimaria^{28,49}, L. Santoro², E. Santovetti³⁷, A. Saputi^{26,49}, D. Saranin⁴⁴, A. Sarnatskiy⁷⁸, G. Sarpis⁵⁹, M. Sarpis⁶³, C. Satriano^{36,s}, A. Satta³⁷, M. Saur⁶, D. Savrina⁴⁴, H. Sazak¹⁷, L.G.Scantlebury Smead⁶⁴, A. Scarabotto¹⁹, S. Schael¹⁷, S. Scherl⁶¹, M. Schiller⁶⁰, H. Schindler⁴⁹, M. Schmelling²¹, B. Schmidt⁴⁹, S. Schmitt¹⁷, H. Schmitz¹⁸, O. Schneider⁵⁰, A. Schopper⁴⁹, N. Schulte¹⁹, S. Schulte⁵⁰, M.H. Schune¹⁴, R. Schwemmer⁴⁹, G. Schwering¹⁷, B. Sciascia²⁸, A. Sciuccati⁴⁹, S. Sellam⁴⁷, A. Semennikov⁴⁴, T. Senger⁵¹, M.Senghi Soares³⁹, A. Sergi²⁹, N. Serra⁵¹, L. Sestini³³, A. Seuthe¹⁹, Y. Shang⁶, D.M. Shangase⁸³, M. Shapkin⁴⁴, R.S. Sharma⁶⁹, I. Shchermerov⁴⁴, L. Shchutska⁵⁰, T. Shears⁶¹, L. Shekhtman⁴⁴, Z. Shen⁶, S. Sheng^{5,7}, V. Shevchenko⁴⁴, B. Shi⁷, Q. Shi⁷, Y. Shimizu¹⁴, E. Shmanin²⁵, R. Shorkin⁴⁴, J.D. Shupperd⁶⁹, R.Silva Coutinho⁶⁹, G. Simi^{33,o}, S. Simone^{24,g}, N. Skidmore⁵⁷, T. Skwarnicki⁶⁹, M.W. Slater⁵⁴, J.C. Smallwood⁶⁴, E. Smith⁶⁵, K. Smith⁶⁸, M. Smith⁶², A. Snoch³⁸, L.Souares Lavra⁵⁹, M.D. Sokoloff⁶⁶, F.J.P. Soler⁶⁰, A. Solomin^{44,55}, A. Solovev⁴⁴, I. Solovyeve⁴⁴, N.S. Sommerfeld¹⁸, R. Song¹, Y. Song⁵⁰, Y. Song^{4,b}, Y.S. Song⁶, F.L.Souza De Almeida⁶⁹, B.Souza De Paula³, E.Spadaro Norella²⁹, E. Spedicato²⁵, J.G. Speer¹⁹, E. Spiridenkov⁴⁴, P. Spradlin⁶⁰, V. Sriskaran⁴⁹, F. Stagni⁴⁹, M. Stahl⁴⁹, S. Stahl⁴⁹, S. Stanislaus⁶⁴, E.N. Stein⁴⁹, O. Steinkamp⁵¹, O. Stenyakin⁴⁴, H. Stevens¹⁹, D. Strelakina⁴⁴, Y. Su⁷, F. Suljik⁶⁴, J. Sun³², L. Sun⁷⁴, D. Sundfeld², W. Sutcliffe⁵¹, P.N. Swallow⁵⁴, K. Swientek⁴⁰, F. Swystun⁵⁶, A. Szabelski⁴², T. Szumlak⁴⁰, Y. Tan^{4,b}, Y. Tang⁷⁴, M.D. Tat⁶⁴, A. Terentev⁴⁴, F. Terzuoli^{15,u,49}, F. Teubert⁴⁹, E. Thomas⁴⁹, D.J.D. Thompson⁵⁴, H. Tilquin⁶², V. Tisserand¹¹, S. T’Jampens¹⁰, M. Tobin^{5,49}, L. Tomassetti^{26,k}, G. Tonani^{30,m,49}, X. Tong⁶, D.Torres Machado², L. Toscano¹⁹, D.Y. Tou^{4,b}, C. Trippel⁴⁵, G. Tuci²², N. Tuning³⁸, L.H. Uecker²², A. Ukleja⁴⁰, D.J. Unverzagt²², B. Urbach⁵⁹, E. Ursov⁴⁴, A. Usachov³⁹, A. Ustyuzhanin⁴⁴, U. Uwer²², V. Vagnoni²⁵, V.Valcarce Cadenas⁴⁷, G. Valenti²⁵, N.Valls Canudas⁴⁹, H.Van Hecke⁶⁸, E. van Herwijnen⁶², C.B.Van Hulse^{47,w}, R.Van Laak⁵⁰, M. van Veghel³⁸, G. Vasquez⁵¹, R.Vazquez Gomez⁴⁶, P.Vazquez Regueiro⁴⁷, C.Vázquez Sierra⁴⁷, S. Vecchi²⁶, J.J. Velthuis⁵⁵, M. Veltri^{27,v}, A. Venkateswaran⁵⁰, M. Verdoggia³², M. Vesterinen⁵⁷, D.Vico Benet⁶⁴, P.V. Vidrier Villalba⁴⁶, M.Vieites Diaz⁴⁹, X. Vilasis-Cardona⁴⁵, E.Vilella Figueras⁶¹, A. Villa²⁵, P. Vincent¹⁶, F.C. Volle⁵⁴, D.vom Bruch¹³, N. Voropaev⁴⁴, K. Vos⁷⁹, C. Vrahas⁵⁹, J. Wagner¹⁹, J. Walsh³⁵, E.J. Walton^{1,57}, G. Wan⁶, C. Wang²², G. Wang⁸, J. Wang⁶, J. Wang⁵, J. Wang^{4,b}, J. Wang⁷⁴, M. Wang³⁰, N.W. Wang⁷, R. Wang⁵⁵, X. Wang⁸, X. Wang⁷², X.W. Wang⁶², Y. Wang⁶, Z. Wang¹⁴, Z. Wang^{4,b}, Z. Wang³⁰, J.A. Ward^{57,1}, M. Waterlaet⁴⁹, N.K. Watson⁵⁴, D. Websdale⁶², Y. Wei⁶, J. Wendel⁸¹, B.D.C. Westhenry⁵⁵, C. White⁵⁶, M. Whitehead⁶⁰, E. Whiter⁵⁴, A.R. Wiederhold⁶³, D. Wiedner¹⁹, G. Wilkinson⁶⁴, M.K. Wilkinson⁶⁶

M. Williams⁶⁵, M.J. Williams⁴⁹, M.R.J. Williams⁵⁹, R. Williams⁵⁶, Z. Williams⁵⁵, F.F. Wilson⁵⁸, M. Winn¹², W. Wislicki⁴², M. Witek⁴¹, L. Witola²², G. Wormser¹⁴, S.A. Wotton⁵⁶, H. Wu⁶⁹, J. Wu⁸, X. Wu⁷⁴, Y. Wu⁶, Z. Wu⁷, K. Wyllie⁴⁹, S. Xian⁷², Z. Xiang⁵, Y. Xie⁸, A. Xu³⁵, J. Xu⁷, L. Xu^{4,b}, L. Xu^{4,b}, M. Xu⁵⁷, Z. Xu⁴⁹, Z. Xu⁷, Z. Xu⁵, K. Yang⁶², S. Yang⁷, X. Yang⁶, Y. Yang^{29,i}, Z. Yang⁶, V. Yeroshenko¹⁴, H. Yeung⁶³, H. Yin⁸, C.Y. Yu⁶, J. Yu⁷¹, X. Yuan⁵, Y. Yuan^{5,7}, E. Zaffaroni⁵⁰, M. Zavertyaev²¹, M. Zdybal⁴¹, F. Zenesini^{25,i}, C. Zeng^{5,7}, M. Zeng^{4,b}, C. Zhang⁶, D. Zhang⁸, J. Zhang⁷, L. Zhang^{4,b}, S. Zhang⁷¹, S. Zhang⁶⁴, Y. Zhang⁶, Y.Z. Zhang^{4,b}, Y. Zhao²², A. Zharkova⁴⁴, A. Zhelezov²², S.Z. Zheng⁶, X.Z. Zheng^{4,b}, Y. Zheng⁷, T. Zhou⁶, X. Zhou⁸, Y. Zhou⁷, V. Zhovkovska⁵⁷, L.Z. Zhu⁷, X. Zhu^{4,b}, X. Zhu⁸, V. Zhukov¹⁷, J. Zhuo⁴⁸, Q. Zou^{5,7}, D. Zuliani^{33,o}, G. Zunica⁵⁰

¹ School of Physics and Astronomy, Monash University, Melbourne, Australia

² Centro Brasileiro de Pesquisas Físicas (CBPF), Rio de Janeiro, Brazil

³ Universidade Federal do Rio de Janeiro (UFRJ), Rio de Janeiro, Brazil

⁴ Department of Engineering Physics, Tsinghua University, Beijing, China

⁵ Institute of High Energy Physics (IHEP), Beijing, China

⁶ School of Physics State Key Laboratory of Nuclear Physics and Technology, Peking University, Beijing, China

⁷ University of Chinese Academy of Sciences, Beijing, China

⁸ Institute of Particle Physics, Central China Normal University, Wuhan, Hubei, China

⁹ Consejo Nacional de Rectores (CONARE), San Jose, Costa Rica

¹⁰ Université Savoie Mont Blanc, CNRS, IN2P3-LAPP Annecy, France

¹¹ Université Clermont Auvergne, CNRS/IN2P3, LPC, Clermont-Ferrand, France

¹² Département de Physique Nucléaire (SPHN), Gif-Sur-Yvette, France

¹³ Aix Marseille Univ, CNRS/IN2P3, CPPM, Marseille, France

¹⁴ Université Paris-Saclay, CNRS/IN2P3, IJCLab, Orsay, France

¹⁵ Laboratoire Leprince-Ringuet, CNRS/IN2P3, Ecole Polytechnique, Institut Polytechnique de Paris, Palaiseau, France

¹⁶ LPNHE, Sorbonne Université, Paris Diderot Sorbonne Paris Cité, CNRS/IN2P3, Paris, France

¹⁷ I. Physikalisches Institut, RWTH Aachen University, Aachen, Germany

¹⁸ Universität Bonn-Helmholtz-Institut für Strahlen und Kernphysik, Bonn, Germany

¹⁹ Fakultät Physik, Technische Universität Dortmund, Dortmund, Germany

²⁰ Physikalisches Institut, Albert-Ludwigs-Universität Freiburg, Freiburg, Germany

²¹ Max-Planck-Institut für Kernphysik (MPIK), Heidelberg, Germany

²² Physikalisches Institut, Ruprecht-Karls-Universität Heidelberg, Heidelberg, Germany

²³ School of Physics, University College Dublin, Dublin, Ireland

²⁴ INFN Sezione di Bari, Bari, Italy

²⁵ INFN Sezione di Bologna, Bologna, Italy

²⁶ INFN Sezione di Ferrara, Ferrara, Italy

²⁷ INFN Sezione di Firenze, Firenze, Italy

²⁸ INFN Laboratori Nazionali di Frascati, Frascati, Italy

²⁹ INFN Sezione di Genova, Genova, Italy

³⁰ INFN Sezione di Milano, Milano, Italy

³¹ INFN Sezione di Milano-Bicocca, Milano, Italy

³² INFN Sezione di Cagliari, Monserrato, Italy

³³ INFN Sezione di Padova, Padova, Italy

³⁴ INFN Sezione di Perugia, Perugia, Italy

³⁵ INFN Sezione di Pisa, Pisa, Italy

³⁶ INFN Sezione di Roma La Sapienza, Roma, Italy

³⁷ INFN Sezione di Roma Tor Vergata, Roma, Italy

³⁸ Nikhef National Institute for Subatomic Physics, Amsterdam, Netherlands

³⁹ Nikhef National Institute for Subatomic Physics and VU University Amsterdam, Amsterdam, Netherlands

⁴⁰ AGH-University of Krakow, Faculty of Physics and Applied Computer Science, Kraków, Poland

⁴¹ Henryk Niewodniczanski Institute of Nuclear Physics Polish Academy of Sciences, Kraków, Poland

⁴² National Center for Nuclear Research (NCBJ), Warsaw, Poland

⁴³ Horia Hulubei National Institute of Physics and Nuclear Engineering, Bucharest-Magurele, Romania

⁴⁴ Affiliated with an institute covered by a cooperation agreement with CERN

⁴⁵ DS4DS, La Salle, Universitat Ramon Llull, Barcelona, Spain

⁴⁶ ICCUB, Universitat de Barcelona, Barcelona, Spain

⁴⁷ Instituto Galego de Física de Altas Enerxías (IGFAE), Universidade de Santiago de Compostela, Santiago de Compostela, Spain

⁴⁸ Instituto de Física Corpuscular, Centro Mixto Universidad de Valencia-CSIC, Valencia, Spain

⁴⁹ European Organization for Nuclear Research (CERN), Geneva, Switzerland

⁵⁰ Institute of Physics, Ecole Polytechnique Fédérale de Lausanne (EPFL), Lausanne, Switzerland

⁵¹ Physik-Institut, Universität Zürich, Zürich, Switzerland

⁵² NSC Kharkiv Institute of Physics and Technology (NSC KIPT), Kharkiv, Ukraine

⁵³ Institute for Nuclear Research of the National Academy of Sciences (KINR), Kyiv, Ukraine

⁵⁴ School of Physics and Astronomy, University of Birmingham, Birmingham, United Kingdom

⁵⁵ H.H. Wills Physics Laboratory, University of Bristol, Bristol, United Kingdom

⁵⁶ Cavendish Laboratory, University of Cambridge, Cambridge, United Kingdom

⁵⁷ Department of Physics, University of Warwick, Coventry, United Kingdom

⁵⁸ STFC Rutherford Appleton Laboratory, Didcot, United Kingdom

⁵⁹ School of Physics and Astronomy, University of Edinburgh, Edinburgh, United Kingdom

⁶⁰ School of Physics and Astronomy, University of Glasgow, Glasgow, United Kingdom

⁶¹ Oliver Lodge Laboratory, University of Liverpool, Liverpool, United Kingdom

⁶² Imperial College London, London, United Kingdom

⁶³ Department of Physics and Astronomy, University of Manchester, Manchester, United Kingdom

⁶⁴ Department of Physics, University of Oxford, Oxford, United Kingdom

⁶⁵ Massachusetts Institute of Technology, Cambridge, MA, United States

⁶⁶ University of Cincinnati, Cincinnati, OH, United States

⁶⁷ University of Maryland, College Park, MD, United States

⁶⁸ Los Alamos National Laboratory (LANL), Los Alamos, NM, United States

⁶⁹ Syracuse University, Syracuse, NY, United States

⁷⁰ Pontifícia Universidade Católica do Rio de Janeiro (PUC-Rio), Rio de Janeiro, Brazil, associated to ³

⁷¹ School of Physics and Electronics, Hunan University, Changsha City, China, associated to ⁸

⁷² Guangdong Provincial Key Laboratory of Nuclear Science, Guangdong-Hong Kong Joint Laboratory of Quantum Matter, Institute of

Quantum Matter, South China Normal University, Guangzhou, China, associated to ⁴

⁷³ Lanzhou University, Lanzhou, China, associated to ⁵

⁷⁴ School of Physics and Technology, Wuhan University, Wuhan, China, associated to ⁴

⁷⁵ Departamento de Física, Universidad Nacional de Colombia, Bogota, Colombia, associated to ¹⁶

⁷⁶ Ruhr Universitaet Bochum, Fakultae f. Physik und Astronomie, Bochum, Germany, associated to ¹⁹

⁷⁷ Eotvos Lorand University, Budapest, Hungary, associated to ⁴⁹

⁷⁸ Van Swinderen Institute, University of Groningen, Groningen, Netherlands, associated to ³⁸

⁷⁹ Universiteit Maastricht, Maastricht, Netherlands, associated to ³⁸

⁸⁰ Tadeusz Kosciuszko Cracow University of Technology, Cracow, Poland, associated to ⁴¹

⁸¹ Universidade da Coruña, A Coruna, Spain, associated to ⁴⁵

⁸² Department of Physics and Astronomy, Uppsala University, Uppsala, Sweden, associated to ⁶⁰

⁸³ University of Michigan, Ann Arbor, MI, United States, associated to ⁶⁹

^a Centro Federal de Educação Tecnológica Celso Suckow da Fonseca, Rio De Janeiro, Brazil

^b Center for High Energy Physics, Tsinghua University, Beijing, China

^c Hangzhou Institute for Advanced Study, UCAS, Hangzhou, China

^d School of Physics and Electronics, Henan University, Kaifeng, China

^e LIP6, Sorbonne Université, Paris, France

^f Universidad Nacional Autónoma de Honduras, Tegucigalpa, Honduras

^g Università di Bari, Bari, Italy

^h Università di Bergamo, Bergamo, Italy

ⁱ Università di Bologna, Bologna, Italy

^j Università di Cagliari, Cagliari, Italy

^k Università di Ferrara, Ferrara, Italy

^l Università di Genova, Genova, Italy

^m Università degli Studi di Milano, Milano, Italy

ⁿ Università degli Studi di Milano-Bicocca, Milano, Italy

^o Università di Padova, Padova, Italy

^p Università di Perugia, Perugia, Italy

^q Scuola Normale Superiore, Pisa, Italy

^r Università di Pisa, Pisa, Italy

^s Università della Basilicata, Potenza, Italy

^t Università di Roma Tor Vergata, Roma, Italy

^u Università di Siena, Siena, Italy

^v Università di Urbino, Urbino, Italy

^w Universidad de Alcalá, Alcalá de Henares, Spain

^x Facultad de Ciencias Físicas, Madrid, Spain

^y Department of Physics/Division of Particle Physics, Lund, Sweden

[†] Deceased